

Probing Evolutionary Population Synthesis Models in the Near Infrared with Early Type Galaxies

Luis Gabriel Dahmer-Hahn^{1,2*}, Rogério Riffel¹, Alberto Rodríguez-Ardila³,
Lucimara P. Martins⁴, Carolina Kehrig⁵, Timothy M. Heckman⁶,
Miriani G. Pastoriza¹, Natacha Z. Dametto¹.

¹*Departamento de Astronomia, Universidade Federal do Rio Grande do Sul. Av. Bento Gonçalves 9500, Porto Alegre, RS, Brazil.*

²*Instituto de Física e Química, Universidade Federal de Itajubá, Brasil.*

³*Laboratório Nacional de Astrofísica - Rua dos Estados Unidos 154, Bairro das Nações. CEP 37504-364, Itajubá, MG, Brazil.*

⁴*NAT - Universidade Cruzeiro do Sul, Rua Galvão Bueno, 868, São Paulo, SP, Brazil.*

⁵*Instituto de Astrofísica de Andalucía, CSIC, Apartado de correos 3004, 18080 Granada, Spain.*

⁶*Center for Astrophysical Sciences, Department of Physics and Astronomy, The Johns Hopkins University, Baltimore, MD 21218, USA.*

Accepted XXX. Received YYY; in original form ZZZ

ABSTRACT

We performed a near-infrared (NIR, $\sim 1.0\mu\text{m}$ - $2.4\mu\text{m}$) stellar population study in a sample of early type galaxies. The synthesis was performed using five different evolutionary population synthesis libraries of models. Our main results can be summarized as follows: low spectral resolution libraries are not able to produce reliable results when applied to the NIR alone, with each library finding a different dominant population. The two newest higher resolution models, on the other hand, perform considerably better, finding consistent results to each other and to literature values. We also found that optical results are consistent with each other even for lower resolution models. We also compared optical and NIR results, and found out that lower resolution models tend to disagree in the optical and in the NIR, with higher fraction of young populations in the NIR and dust extinction ~ 1 magnitude higher than optical values. For higher resolution models, optical and NIR results tend to agree much better, suggesting that a higher spectral resolution is fundamental to improve the quality of the results.

Key words: galaxies: stellar content – stars: AGB and post-AGB – infrared: galaxies

1 INTRODUCTION

Understanding the processes involved in galaxy evolution is one of the main topics of modern astrophysics. These processes are mainly driven by the star formation history (SFH) of the galaxies. One of the main methods to access the unresolved stellar content of galaxies is by comparing their observed spectra with combinations of simple stellar population (SSPs) libraries. These libraries can be empirical (in this case being limited by the properties of nearby stellar clusters) or can be constructed by using knowledge about stellar evolution, a technique called evolutionary population synthesis (EPS, e.g. Bruzual & Charlot 2003; Maraston 2005; Conroy et al. 2009; Meneses-Goytia et al. 2015; Röck et al.

2016, hereafter BC03, M05, C09, MG15 and MIUSCAT, respectively).

The SSPs are usually constructed using one of the two alternatives: isochrone synthesis or “fuel consumption based” algorithms. With the first approach, SSPs are calculated by integrating the stellar contributions to the flux in the various pass-bands of all mass-bins along one isochrone, after assuming an Initial Mass Function (IMF, e.g. BC03). In the second approach, after leaving the main sequence, the duration of each subsequent phase in stellar evolution is calculated by using the fuel consumption theory (e.g. M05).

The big problem is that both approaches result in very different luminosities for short evolutionary stages, especially the crucial TP-AGB phase, whose underlying physics is still poorly known (M05, Marigo et al. 2008; Conroy & Gunn 2010; Conroy 2013; Kriek et al. 2010; Zibetti et al. 2013; Noël et al. 2013; Riffel et al. 2015). This happens be-

* E-mail: dahmer.hahn@ufrgs.br

cause some processes of stellar evolution (mass-loss, changing opacities, dredge-up events, etc.) are not well understood, and receive a different treatment in each model flavour (e.g. BC03, M05, C09, MG15 and MIUSCAT). Models based on the fuel consumption theory tend to overpredict TP-AGB features while those based on isochrone synthesis generally underestimate them (Zibetti et al. 2013, and references therein), although a few models based on isochrone synthesis also contain large amounts of these stars (e.g. Marigo et al. 2008). Currently, there is no consensus regarding what TP-AGB contribution best reproduces the observed spectra of galaxies. Many stellar absorption features predicted by TP-AGB heavy models have been found, like the $1.1 \mu\text{m}$ CN band (Riffel et al. 2007), the $1.4 \mu\text{m}$ CN band (Martins et al. 2013) and the ZrO features at $0.8\text{--}1.0 \mu\text{m}$ (Martins et al. 2013). On the other hand, Zibetti et al. (2013) did not detect the TP-AGB spectral features predicted by M05 in their spectra of post-starburst galaxies at $z \sim 0.2$. Riffel et al. (2015) found that models based on empirical libraries that predict relatively strong near infrared (NIR) features provide a more accurate description of the data. However, none of the models tested by them successfully reproduces all of the features observed in the spectra. Also, Riffel et al. (2015) claimed that stars in other evolutionary phases like RGB may be crucial to describe the absorption features detected in galaxies and that empirical spectra of these kind of stars should be included in the EPS models.

The libraries of SSPs are then used by a computing code (e.g. STARLIGHT, Cid Fernandes et al. 2005) to determine parameters such as ages, element abundances, stellar masses and stellar mass functions by searching for the combination of SSPs that best reproduces the observed spectrum.

A major issue when characterizing the stellar population of a galaxy is attributed to the dependence of results in the model set used when fitting the underlying stellar features (Chen et al. 2010). This happens because of all the uncertainties related to the construction of the SSPs. Summed to these effects, there is the well known age-metallicity degeneracy, which difficults to distinguish between an old stellar population and a reddened or more metallic younger one (Worthey 1994).

Here we aim to compare, for the first time in the literature, the stellar population predictions derived using NIR spectra of different sets of EPS models for the central region of 6 local early-type galaxies (ETGs) and one spiral galaxy. The former morphological type was chosen because it contains a relatively homogeneous old stellar population. We are aware, though, that current day interpretation is that these objects experienced moderately different star formation histories, with the present-day stellar populations slightly differing in metallicity and/or age (Rickes et al. 2009, and references therein).

This paper is structured as follows: The data and reduction process are presented in Section 2. The Stellar Population Synthesis method used in the analysis is presented in Section 3. In Section 4, we present the main results from the synthesis using the different sets of SSPs. A discussion of these results is in Section 5. The final remarks are given in section 6.

2 DATA AND REDUCTION

From the 6 ETGs, 5 are from the Calar Alto Legacy Integral Field Area Survey (CALIFA Sánchez et al. 2012; Walcher et al. 2014; Sánchez et al. 2016). These objects were selected for being the ETGs in the CALIFA data release 1 and accessible to the night sky during the observing run. Also, the CALIFA papers confirmed the presence of warm gas for these 5 galaxies. The final 7 targets were selected on the basis of surface brightness to offer a good compromise between S/N and exposure time. We also observed NGC 4636, a typical LINER, and NGC 5905, classified as SB(r)b, for comparison. The infrared data were obtained at the Astrophysical Research Consortium (ARC) telescope. The Triple-Spec (Wilson et al. 2004) instrument was used to obtain cross-dispersed spectra in the range $0.95\text{--}2.46 \mu\text{m}$. We used the $1.1''$ slit, resulting in a spectral resolution of $R \sim 2000$. After each target, we observed an A0V, A1V or A2V star at a similar airmass for flux calibration and telluric correction. Both the science objects and the telluric stars were observed following the dithering pattern object-sky-object. Internal flat-field and arc lamp exposures were also acquired for pixel response and wavelength calibration, respectively. The reduction of the data was done using Triplespectool, a modified version of Spextool (Vacca et al. 2004; Cushing et al. 2004) using standard settings. These spectra are available for download at the MNRAS website.

Table 1 shows the basic properties for the sample. Also, in order to compare NIR results with optical ones, for the five CALIFA objects, we extracted optical spectra using apertures of size similar to that of the NIR slit. For NGC 4636, which is not within the CALIFA targets, we used optical spectra from SDSS. Figure 1 shows Two Micron All Sky survey (2MASS) JHK imaging of the sample with the slit orientation. The individual description of the objects of the sample is presented in the Appendix A. Optical and NIR spectra are shown in Figure 2 and Figure 3, respectively.

3 STELLAR POPULATION SYNTHESIS

The stellar population synthesis technique consists basically of comparing the observed spectrum of a galaxy with a combination of SSPs with different ages and metallicities (this set of SSPs is known as a base of elements, Cid Fernandes et al. 2005), searching for a combination of SSPs that suitably fits the observed spectrum.

For a proper fitting of a galaxy's stellar population, the library of models must cover the range of possible observed spectral properties (e.g. ages and metallicities). It is also fundamental to choose an adequate number of elements for such library in order to have non-degenerate solutions (Schmidt et al. 1991; Cid Fernandes et al. 2005; Dametto et al. 2014). Chen et al. (2010), presented a study in the optical region showing that different models may result in quite different SFHs for the same observed spectrum. Studying six different types of galaxies (star-forming galaxies, composite galaxies, Seyfert 2s, LINERs, E+A, and early-type galaxies) using 6 different EPS models, they found that the differences found are significant, but the dominant populations are unaltered. Also, they found that using the same models, the results depend on the selected ages. In the NIR, this scenario seems

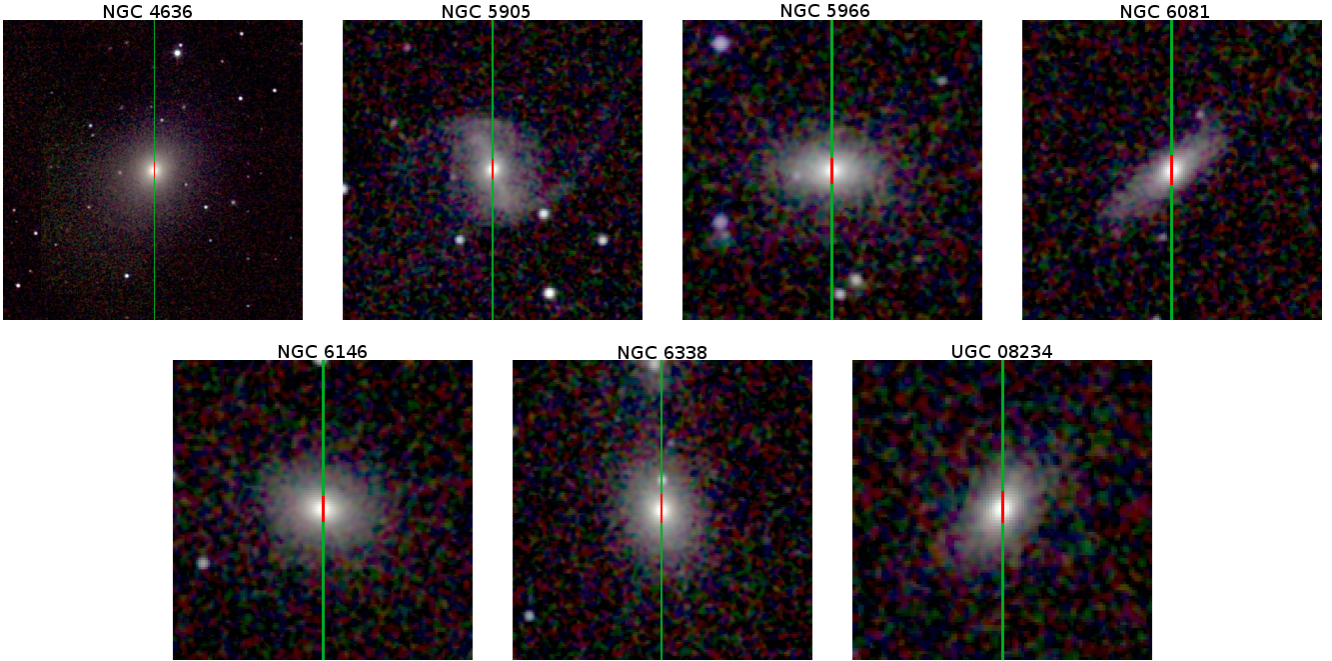


Figure 1. Combined 2MASS JHKs imaging for the galaxy sample. The vertical green line shows the slit orientation while the red segment indicates the aperture used to extract the spectra.

Table 1. Basic properties for the sample.

Object	Morphology ¹	K magnitude ²	Absolute K magnitude ³	z ⁴	Aperture Radius (arcsec)	Exposure Time (min)	S/N ⁵	Optical ⁶ spectrum
NGC 4636	E0-1	9.0	-21.6	0.003129	10.0	27.0	54	SDSS
NGC 5905	SB(r)b	11.0	-22.4	0.011308	7.0	24.0	30	—
NGC 5966	E	10.7	-23.3	0.014924	6.0	24.0	24	CALIFA
NGC 6081	S0	10.5	-23.8	0.017265	6.0	36.0	45	CALIFA
NGC 6146	E?	10.3	-25.2	0.029420	3.0	36.0	56	CALIFA
NGC 6338	S0	10.6	-24.7	0.027427	4.0	36.0	30	CALIFA
UGC 08234	S0/a	10.7	-24.6	0.027025	6.0	36.0	32	CALIFA

Table Notes: ¹ de Vaucouleurs et al. (1991) ² Two Micron All Sky survey team, 2003, 2MASS extended objects, final release ³ Calculated based in the apparent magnitude and the redshift and assuming $H=70 \text{ km s}^{-1} \text{ Mpc}^{-1}$ ⁴ NED ⁵ K-band Signal-to-Noise ratio before smoothing the spectra. ⁶ Presence or absence of SDSS spectra.

to be more dramatic, since the inclusion of the TP-AGB phase in the models is still very uncertain and is a matter of debate (M05, Marigo et al. 2008; Conroy & Gunn 2010; Conroy 2013; Kriek et al. 2010; Zibetti et al. 2013; Noël et al. 2013; Riffel et al. 2015). To properly address this issue we decided to build eight different libraries of models using five different EPS models flavours, as follows:

- i. Bruzual & Charlot (2003, BC03)
- ii. Maraston (2005, M05)
- iii. Conroy et al. (2009, C09)
- iv. Meneses-Goytia et al. (2015, MG15)
- v. Röck et al. (2016, MIUSCAT)

Details of the EPS models, as well as the chosen ages, metallicities and evolutionary tracks of the SSPs used in the fitting are listed in Table 2. Since MG15 and MIUSCAT have only SSPs with ages $t \geq 1 \text{ Gyr}$, in order to allow for a suitable

comparison of the results from the different EPS models, we created 3 additional libraries of models by removing the SSPs with ages $t < 1 \text{ Gyr}$ from BC03, M05 and C09 models. These libraries do not include SSPs younger than 1Gyr because of the lack of hot stars in the IRTF library (Cushing et al. 2005; Rayner et al. 2009), which was used to build the models.

It is worth mentioning that in the NIR, the spectral resolution of BC03, M05 and C09 is lower than that of the observed spectra. We then rebinned the data in order to match the spectral resolution of the models. Considering that MG15 and MIUSCAT have a spectral resolution similar to that of the observed spectra, this procedure was not necessary when these later libraries were employed.

Regarding TP-AGB treatment, BC03 uses low-resolution stellar templates from Höfner et al. (2000), while M05 and C09 use higher resolution TP-AGB spectra from

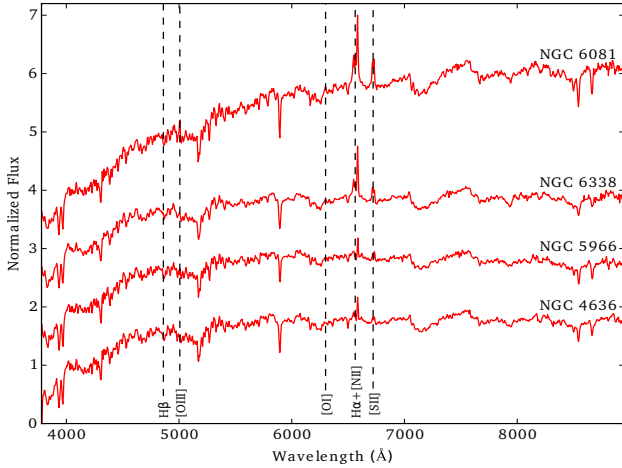


Figure 2. Red curves represent SDSS spectra, which are available for four galaxies of the sample. Rest-frame wavelengths of the main optical emission-lines are indicated.

Lançon & Mouhcine (2002), degrading them to match the rest of the spectra. MG15 and MIUSCAT use the IRTF library, which also contains TP-AGB stars (Riffel et al. 2015).

Since our objects may host a low-luminosity AGN (LLAGN), we followed Riffel et al. (2009, and references therein). In addition, we added to the base set a power law with $F_\nu \propto \nu^{-1.5}$ to represent the featureless continuum (FC) emission from the AGN. Moreover, in the NIR, 8 planck distributions with temperatures from 700 to 1400 K were also added, in steps of 100 K. They represent hot dust continuum heated by the AGN (see Riffel et al. 2009).

3.1 Fitting Procedures

In order to fit the stellar populations, we used the STARLIGHT code, which is described in Cid Fernandes et al. (2004, 2005). In summary, the code fits the observed spectrum with a combination of SSPs in different proportions. It also searches for the internal extinction that best describes the observed spectrum. To this aim, we used the Cardelli et al. (1989) reddening law. Basically, by using a χ^2 minimization approach, STARLIGHT fits an observed spectrum O_λ with a combination of N_\star SSPs solving the equation:

$$M_\lambda = M_{\lambda 0} \left[\sum_{j=1}^{N_\star} x_j b_{j,\lambda} r_\lambda \right] \otimes G(v_\star, \sigma_\star)$$

where M_λ is a model spectrum, $M_{\lambda 0}$ is the flux at the normalized point λ_0 , N_\star is the number of SSPs used to compose the model, \vec{x} is the population vector so that x_j indicates the contribution from the j -esim SSP normalized at λ_0 , $b_{j,\lambda}$ is the j -esim model spectrum, r_λ is the reddening factor $r_\lambda = 10^{-0.4(A_\lambda - A_{\lambda_0})}$, which is parameterized by the dust extinction, A_ν . The stellar velocity dispersions and group velocities are modelled by a gaussian function $G(v_\star, \sigma_\star)$.

4 RESULTS

The upper panels of figs. 4 to 10 show, for each galaxy of the sample, the observed (black) and modeled (red) spectra for each of the 8 libraries of models employed. Areas with high atmospheric absorption were shaded in the Figures. The bottom panels show in blue the luminosity contributions (metallicities summed) for every age of the best model fitted by STARLIGHT.

Since small differences in the ages of the stellar populations are washed away by the noise present in real data, a more consistent and robust way to present the results is in the form of condensed population vectors (Cid Fernandes et al. 2004, 2005). With this in mind, we followed Riffel et al. (2009) and defined the light fraction population vectors as follows: x_y ($t \leq 50\text{Myr}$), x_i ($50\text{Myr} < t \leq 2\text{Gyr}$) and x_o ($t > 2\text{Gyr}$) to represent the young, intermediate and old stellar population vectors, respectively. The same age bins were used for the mass fraction population vectors. Besides, we defined cold and hot dust emission vectors, BB_c for $T \leq 1000\text{K}$ and BB_h for $T > 1000\text{K}$. The results for these binned population vectors for each galaxy are presented in Table 3.

We also followed Cid Fernandes et al. (2005), who proposed two additional parameters to describe the SP mixture of a galaxy. These parameters are the mean stellar age ($\langle t \rangle$) and mean metallicity ($\langle Z \rangle$), which are defined by the following equations

$$\langle t \rangle_L = \sum_{j=1}^{N_\star} x_j \log(t_j)$$

$$\langle Z \rangle_L = \sum_{j=1}^{N_\star} x_j Z_j$$

where t_j and Z_j are the age and metallicity of the j -esim SSP. The x_j percentage contribution can be weighted by light (L) and mass (M) fractions. These parameters, together with the AdeV, are also listed in Table 3 (AdeV is a value that measures the fit quality, according to the relation $|O_\lambda - M_\lambda|/O_\lambda$). For a better visualization of the trends on each library of models, we summed the percentage contribution of the 7 objects and presented them on Fig 11.

Fits performed with the BC03 library of models display higher contribution from young populations, a mild contribution from old populations, no contribution of intermediate-age populations and a higher A_v when compared with the other models. With M05, the sample shows a dominance of intermediate age populations, with significant amounts of young and old populations. When using C09 library, STARLIGHT finds a dominance of old stellar populations, with mild contribution from young populations. When using low resolution models that do not include young populations, BC03io and C09io models result in a $\sim 97\%$ contribution from old populations for all the objects, with the other 3% due to the FC+BB. When using M05io models, on the other hand, 3 objects (NGC 4636, NGC 5905 and NGC 6081) appear dominated by intermediate age populations, with old populations dominating the rest of the sample. With high spectral resolution libraries of models, a dominance of old populations was found, with higher contributions from FC and BB when compared with lower resolution ones. However, results obtained using MIUSCAT library display a trend to

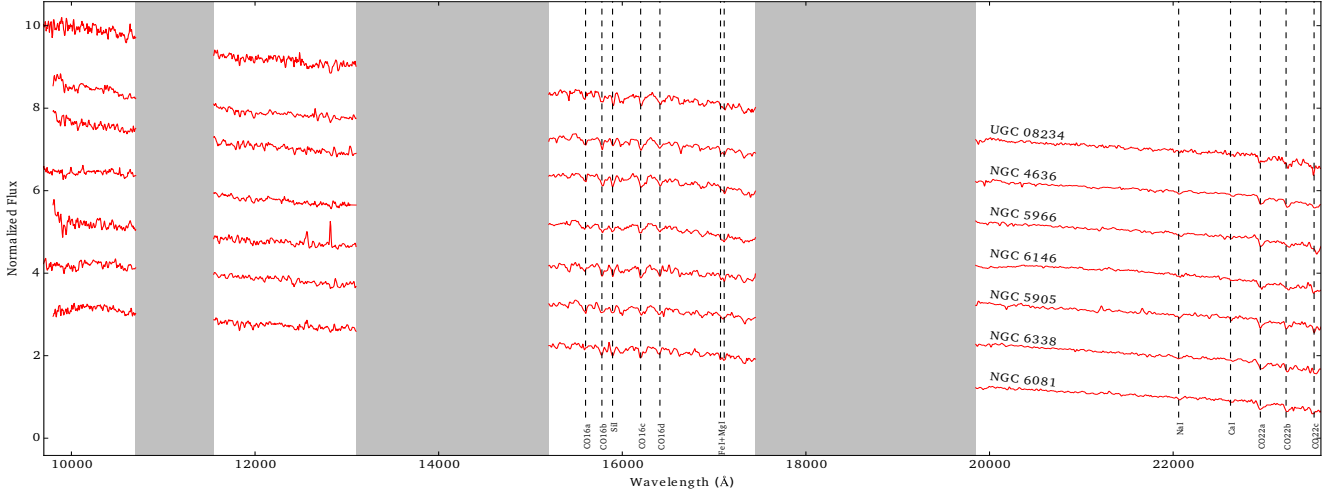


Figure 3. NIR spectra for the sample. The main absorption bands are indicated by dashed lines. High telluric absorption regions are shaded.

Table 2. Basic properties for the EPS models and informations on the used SSPs.

SSP	Ages (Gyr)	Metallicities (Z_{\odot})	Spectral resolution (Optical/NIR)	Stellar Library	IMF	Evolutionary Track
BC03	0.001, 0.0031, 0.0050, 0.0066, 0.0087, 0.01, 0.014, 0.025, 0.04, 0.055, 0.1, 0.16, 0.28, 0.50, 0.9, 1.27, 1.43, 2.5, 4.25, 6.25, 7.5, 10, 13 and 15	0.005, 0.02, 0.2, 0.4, 1, 2.5	2000/300	STELIB ¹ / BaSeL 3.1 ²	Salpeter ³	Padova ⁴
BC03io	1.27, 1.43, 2.5, 4.25, 6.25, 7.5, 10, 13 and 15	0.005, 0.02, 0.2, 0.4, 1, 2.5	2000/300	STELIB/ BaSeL 3.1	Salpeter	Padova
M05	0.001, 0.003, 0.0035, 0.004, 0.005, 0.0055, 0.006, 0.0065, 0.007, 0.0075, 0.008, 0.0085, 0.009, 0.01, 0.015, 0.02, 0.025, 0.03, 0.05, 0.08, 0.2, 0.03, 0.04, 0.05, 0.07, 0.08, 1.0, 1.5, 2.0, 3.0 and 13	0.02, 0.5, 1 and 2	300/300	BaSeL 2.2 ²	Salpeter	Cassisi ⁵ + Geneva ⁶
M05io	1.0, 1.5, 2.0, 3.0 and 13	0.02, 0.5, 1 and 2	300/300	BaSeL 2.2	Salpeter	Cassisi + Geneva
C09	0.00032, 0.00075, 0.0025, 0.0035, 0.004, 0.0044, 0.005, 0.0056, 0.0063, 0.0075, 0.0079, 0.0084, 0.0089, 0.016, 0.032, 0.038, 0.045, 0.063, 0.071, 0.089, 0.21, 0.32, 0.42, 0.53, 0.89, 2.11, 5.31, 6.31, 8.91 and 12.59	0.02, 0.3, 0.95 and 1.5	300/300	BaSeL 3.1	Salpeter	Padova
C09io	2.11, 5.31, 6.31, 8.91 and 12.59	0.02, 0.3, 0.95 and 1.5	300/300	BaSeL 3.1	Salpeter	Padova
MG15	1.0, 1.12, 1.26, 1.41, 1.58, 1.78, 2.0, 2.24, 2.51, 2.82, 3.16, 3.55, 3.98, 4.47, 5, 5.62, 6.31, 7, 7.94, 8.91, 10, 11.2, 12.6 and 14.1	0.0038, 0.0076, 0.019 and 0.03	—/2000	IRTF ⁷	Salpeter	Padova
MIUSCAT	1.0, 1.25, 1.5, 1.75, 2.0, 2.25, 2.5, 2.75, 3.0, 3.25, 3.5, 3.75, 4.0, 4.5, 5.0, 5.5, 6.0, 6.5, 7.0, 7.5, 8.0, 8.5, 9.0, 9.5, 10.0, 10.5, 11.0, 11.5, 12.0, 12.5, 13.0, 13.5 and 14.0	0.0085, 0.01, 0.022, 0.027	—/2000	IRTF	Revised Kroupa ⁸	BaSTI ⁹

Table Notes: (1) Le Borgne et al. (2003) (2) Lejeune et al. (1997, 1998); Westera et al. (2002) (3) Salpeter (1955) (4) Marigo et al. (2008) and references therein (5) Cassisi et al. (1997b,a) (6) Schaller et al. (1992) (7) Cushing et al. (2005); Rayner et al. (2009) (8) Kroupa (2001) (9) Pietrinferni et al. (2004)

ward intermediate-age SSPs whereas results obtained using MG15 library display a trend toward old SSPs. For NGC 6338 and UGC 08234, STARLIGHT found intermediate-age populations dominating the emission (70% and 54 % respectively) when using MIUSCAT library, while no contribution was found when using MG15. For NGC 5905, a contribution of 31% from an intermediate population was found when using MIUSCAT library, while no contribution was found for this age when using MG15. For a better visualization of these differences, we plotted the average contribution from

young, intermediate and old populations plus the summed contributions of the FC and BB on Figure 11

The stellar synthesis using low spectral resolution libraries of models did not fit properly the $2.3\mu\text{m}$ CO bands on NGC 5966, NGC 6146, NGC 6338 and UGC 08234 regardless of the low resolution library of models used. The NaI and CaI lines in the K-band and the absorptions in the J and H band were not fitted with any low resolution library. A similar result was reported by Riffel et al. (2015), who found that none of the models tested by them (BC03, M05 and Maraston & Strömbäck 2011) accurately repro-

Table 3. Results for the NIR synthesis.

Library	FC1.50	BB _c	BB _h	xy	xi	xo	my	mi	mo	Av	$\langle t \rangle_L$	$\langle Z \rangle_L$	Adev
NGC 4636													
BC03	0.0	0.0	0.0	56.8	2.0	41.0	5.7	0.8	93.4	1.52	8.49	0.01796	1.34
M05	0.0	0.0	0.0	26.1	57.1	16.7	1.4	51.1	47.3	1.12	8.58	0.02362	1.05
C09	0.0	0.0	0.0	30.1	0.0	69.9	—	—	—	1.33	8.91	0.01439	1.27
BC03io	0.0	0.0	0.0	0.0	0.0	100.0	0.0	0.0	100.0	1.23	9.90	0.01679	1.86
M05io	0.0	0.0	0.0	0.0	60.2	39.7	0.0	40.0	59.9	1.02	9.36	0.02579	1.08
C09io	0.0	0.0	0.0	0.0	0.0	100.0	—	—	—	1.11	9.84	0.009632	1.54
MG15	0.0	0.0	6.4	0.0	0.0	93.5	—	—	—	0.27	9.82	0.02089	1.50
MIUSCAT	0.0	0.0	6.7	0.0	0.0	93.2	—	—	—	0.57	9.91	0.01624	1.85
NGC 5905													
BC03	4.2	0.0	0.0	59.4	6.6	29.7	4.4	3.0	92.5	2.12	8.16	0.02282	1.28
M05	3.6	0.0	0.0	43.7	43.7	8.8	3.3	39.9	56.7	1.96	8.18	0.02438	1.02
C09	0.0	0.0	0.0	53.4	16.1	30.4	—	—	—	2.38	8.11	0.02211	1.08
BC03io	8.2	0.0	0.0	0.0	0.3	91.3	0.0	0.4	99.5	1.43	9.44	0.02104	1.85
M05io	5.6	0.0	0.0	0.0	51.5	42.8	0.0	34.9	65.0	1.58	9.38	0.02081	1.21
C09io	7.7	0.0	0.0	0.0	0.0	92.2	—	—	—	1.74	9.75	0.006616	1.56
MG15	13.3	0.0	0.0	0.0	0.0	86.6	—	—	—	0.93	10.06	0.005964	1.59
MIUSCAT	4.5	4.0	0.0	0.0	31.0	60.3	—	—	—	1.10	9.76	0.01444	1.63
NGC 5966													
BC03	0.0	0.0	0.0	72.5	0.0	27.4	12.5	0.0	87.5	1.70	8.31	0.0146	1.85
M05	0.0	0.0	0.0	25.4	23.3	51.2	0.8	4.5	94.6	1.54	8.70	0.01968	2.12
C09	0.0	0.0	0.0	0.0	0.0	100.0	—	—	—	1.41	10.01	0.002981	2.02
BC03io	0.0	0.0	0.0	0.0	0.0	100.0	0.0	0.0	100.0	1.29	9.78	0.01137	2.54
M05io	0.0	0.0	0.0	0.0	21.6	78.3	0.0	6.2	93.7	1.41	9.71	0.0157	2.20
C09io	0.0	0.0	0.0	0.0	0.0	100.0	—	—	—	1.42	10.02	0.003037	2.01
MG15	0.0	0.0	0.0	0.0	0.0	100.0	—	—	—	0.77	10.15	0.006124	2.11
MIUSCAT	0.0	0.0	0.0	0.0	0.0	100.0	—	—	—	0.53	10.12	0.02184	2.01
NGC 6081													
BC03	0.0	0.0	0.0	50.2	0.0	49.7	4.3	0.0	95.6	1.85	8.76	0.02432	0.94
M05	0.0	0.0	0.0	8.2	48.1	43.6	0.2	19.2	80.5	1.66	9.28	0.02499	0.97
C09	0.0	0.0	0.0	25.0	0.0	74.9	—	—	—	1.87	9.13	0.01255	1.04
BC03io	0.0	0.0	0.0	0.0	0.0	100.0	0.0	0.0	100.0	1.62	9.85	0.02028	1.28
M05io	0.0	0.0	0.0	0.0	52.9	47.0	0.0	23.8	76.2	1.61	9.52	0.02437	1.00
C09io	0.0	0.0	0.0	0.0	0.0	100.0	—	—	—	1.80	9.92	0.01291	1.06
MG15	0.0	2.3	0.0	0.0	0.0	97.6	—	—	—	1.04	10.07	0.0131	1.31
MIUSCAT	0.0	3.6	0.0	0.0	0.0	96.3	—	—	—	0.90	10.11	0.02622	1.34
NGC 6146													
BC03	0.0	0.0	0.0	48.7	0.0	51.2	1.1	0.0	98.8	1.28	8.61	0.01962	1.88
M05	0.0	0.0	0.0	32.6	41.1	26.2	0.7	20.5	78.7	1.00	8.64	0.03	1.73
C09	0.0	0.0	0.0	55.3	9.9	34.7	—	—	—	1.42	8.17	0.02094	1.72
BC03io	7.0	0.0	0.1	0.0	0.0	92.8	0.0	0.0	100.0	0.75	9.77	0.01976	2.15
M05io	0.0	0.0	3.9	0.0	40.8	55.2	0.0	13.9	86.0	0.77	9.34	0.03544	1.77
C09io	0.0	0.0	5.5	0.0	0.0	94.4	—	—	—	0.88	10.03	0.01448	2.30
MG15	0.0	0.0	8.4	0.0	18.1	73.4	—	—	—	0.14	9.44	0.006848	2.00
MIUSCAT	0.0	0.0	12.4	0.0	17.8	69.7	—	—	—	0.22	9.51	0.02177	2.34
NGC 6338													
BC03	0.00	0.00	0.00	72.3	0.00	27.6	10.2	0.0	89.7	1.49	8.21	0.02373	1.86
M05	0.00	0.00	0.00	54.8	39.4	5.7	6.4	35.2	58.2	1.79	7.82	0.02323	2.12
C09	0.00	0.00	0.00	6.83	13.3	79.7	—	—	—	1.70	9.65	0.003544	2.16
BC03io	0.00	0.00	0.00	0.00	0.00	100.0	0.0	0.0	100.0	1.18	9.50	0.0243	2.23
M05io	0.00	0.00	0.00	0.00	45.7	54.2	0.0	22.4	77.5	1.56	9.37	0.01852	2.25
C09io	0.00	0.00	0.00	0.00	0.00	100.0	—	—	—	1.57	9.96	0.0004	2.09
MG15	1.8	0.00	0.00	0.00	0.00	98.1	—	—	—	0.88	10.13	0.005994	1.76
MIUSCAT	0.7	0.00	0.00	0.00	18.2	81.0	—	—	—	0.97	9.93	0.0119	1.75
UGC 08234													
BC03	0.0	0.0	0.0	67.8	0.0	32.1	6.5	0.0	93.4	0.89	8.22	0.02292	1.48
M05	0.0	0.0	0.0	46.3	43.0	10.6	4.1	32.2	63.5	0.83	7.95	0.02678	1.41
C09	0.0	0.0	0.0	27.1	0.0	72.8	—	—	—	0.91	9.06	0.01242	1.68
BC03io	0.0	0.0	0.0	0.0	0.0	100.0	0.0	0.0	100.0	0.64	9.90	0.01971	1.74
M05io	0.0	0.0	0.0	0.0	47.7	52.2	0.0	21.6	78.3	0.62	9.42	0.02828	1.59
C09io	0.0	0.0	0.0	0.0	0.0	100.0	—	—	—	0.75	9.89	0.01307	1.77
MG15	0.0	0.0	0.0	0.0	0.0	100.0	—	—	—	0.17	9.88	0.01127	1.94
MIUSCAT	0.0	0.0	0.0	0.0	54.4	45.5	—	—	—	0.21	9.61	0.01744	2.11

duces all of the stellar features observed in the spectra. In all cases, the fits improved when young populations were included. When using high resolution libraries, the absorption features in H and K bands were fitted with a much better agreement between models and observations. However, in the J band, because of the low signal-to-noise ratio, the fits are not as good. Note that this is not a big issue because this band is mostly used for fitting the continuum inclination.

5 DISCUSSION

5.1 NIR models with low spectral resolution

Our sample is composed mainly of ETGs (NGC 4636, NGC 5966, NGC 6081, NGC 6146, NGC 6338 and UGC 08234), which are mainly constituted of old populations (Rickes et al. 2009, and references therein). Analysing Table 3, it is clear that for libraries of models with low spectral resolution (BC03, M05 and C09), the results are linked to the library used rather than to the galaxy properties themselves. This result is different from the optical result reported by Chen et al. (2010). They found that changing the library would result in a change of the percentage contributing light fractions, even though the dominant populations are unaltered. They also compared high and low resolution libraries, and the dominant populations still remained unchanged. This is not the case for the NIR. We found from figs. 4 to 10 (see also Table 3) that for the NIR spectral range, the dominant population is highly dependent on the chosen models.

According to our results, BC03 models give the highest contribution from young populations in the whole sample. The higher young SP contributions are also linked to a higher reddening value, as we can see from Table 3. This result is in agreement with those found by Riffel et al. (2015). However, they are in contrast with the ones reported by Capozzi et al. (e.g. 2016), who found that the inclusion of TP-AGB stars tend to produce results with older ages. This difference might be connected to the fact that they used panchromatic Spectral Energy Distributions, while we used only NIR spectra to make the comparison.

Indeed, for models with low spectral resolution, the large variation in age when young populations are not included implies that the synthesis is unable to distinguish between an old population and a reddened younger one or a more metallic one, since in all cases, the younger populations are followed by a higher extinction or a higher metallicity. This result was first discussed by Worthey (1994) and seems to still hold in the NIR.

Regarding the metallicity, when young populations are present in the fitting process, both BC03 and M05 find values close to solar. C09, on the other hand, tends to find subsolar values of metallicity. When young ages are removed, the same results still hold. Concerning the high resolution libraries, MIUSCAT also finds values close to Z_{\odot} whereas MG15, tends to find subsolar values.

Also, all model sets with low spectral resolution found high ($A_V \gtrsim 1.0$ mag) values of extinction. These results are incompatible with literature results who show that ETGs have negligible amounts of dust (Padilla & Strauss 2008).

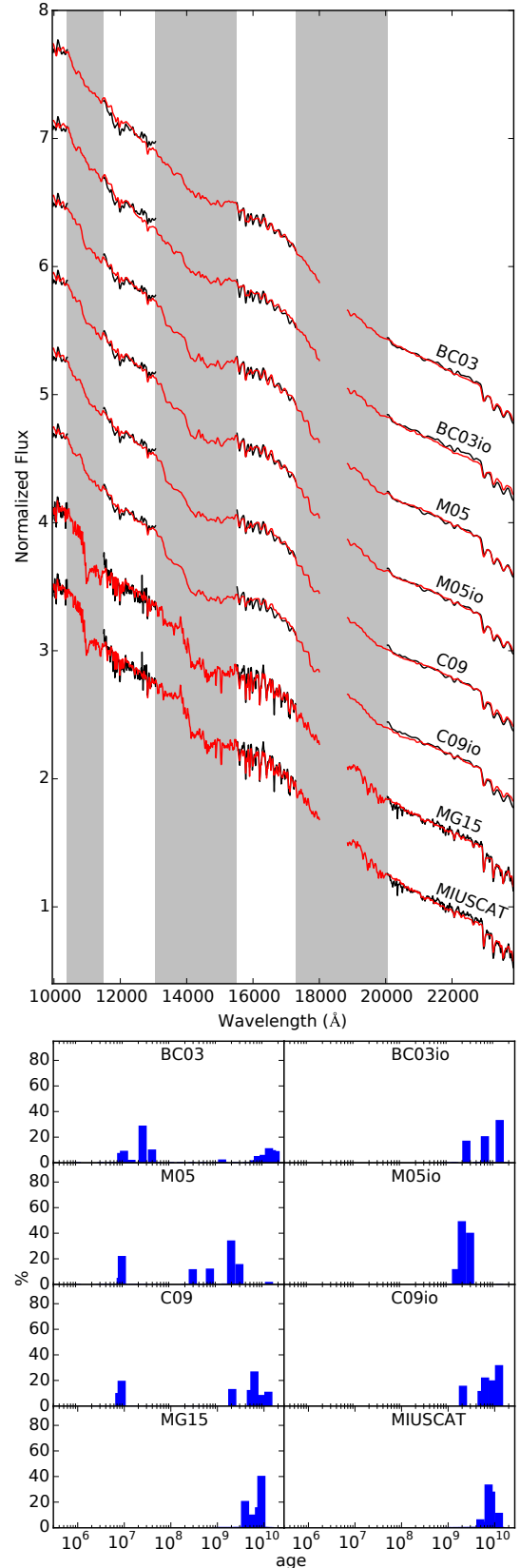


Figure 4. NIR results for NGC 4636 using the 8 libraries of models. On the upper panel, observed spectrum is shown in black and modelled spectrum is shown in red. Masked areas are shaded. On the bottom panel, we show in blue the percentage luminosity contribution for every age.

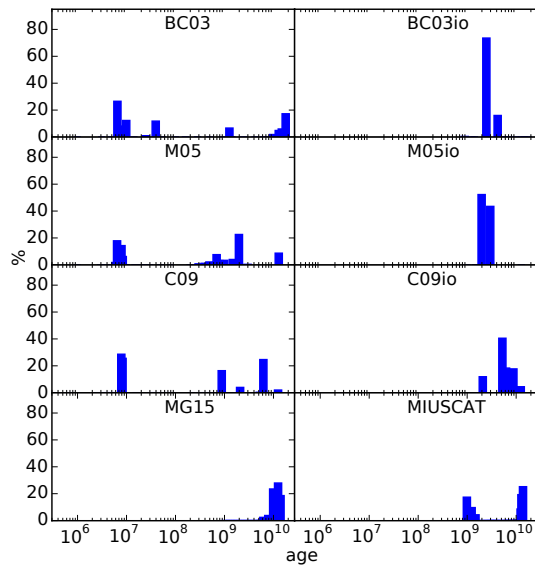
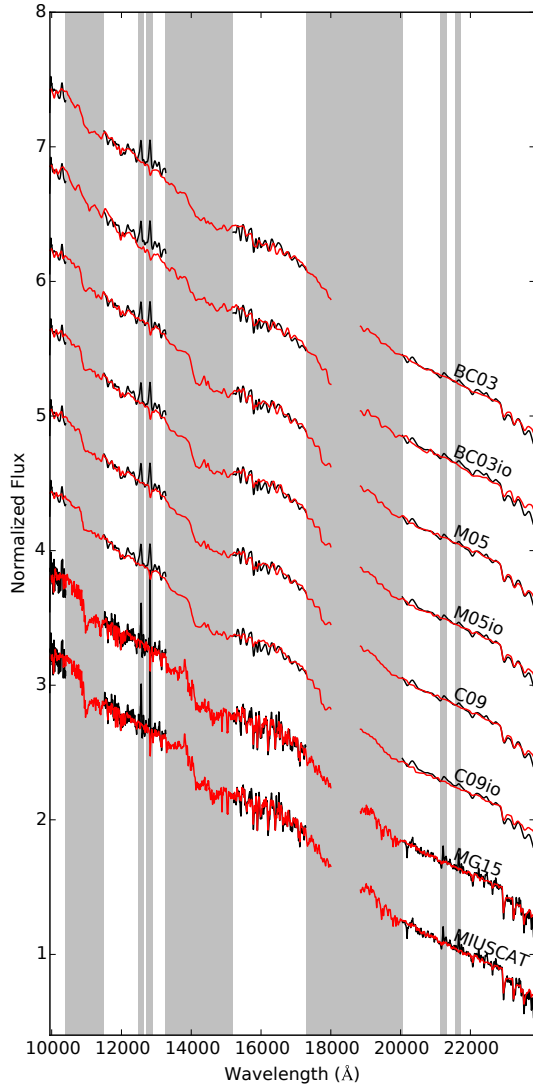


Figure 5. Same as Figure 4 for NGC 5905. Emission lines are also shaded on the upper panel.

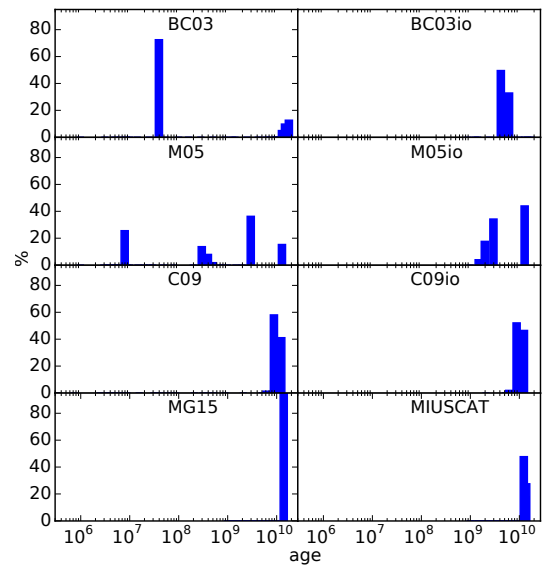
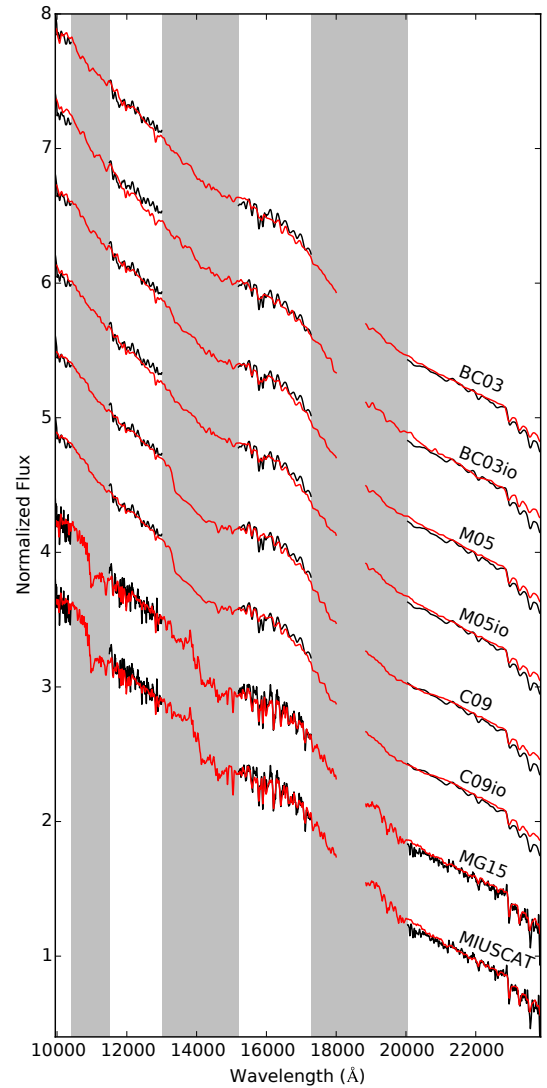


Figure 6. Same as Figure 4 but for NGC 5966

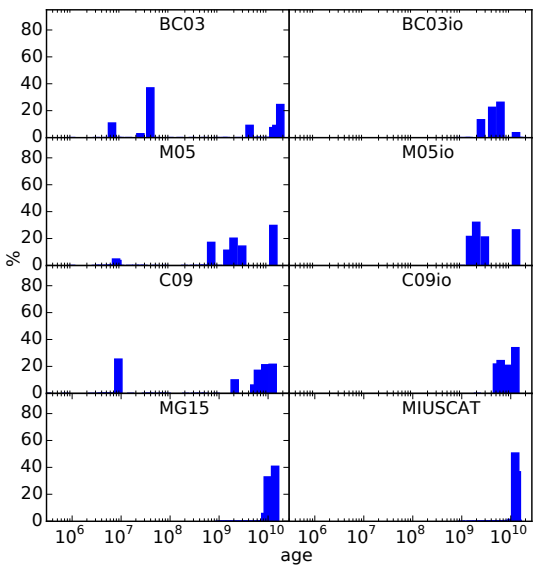
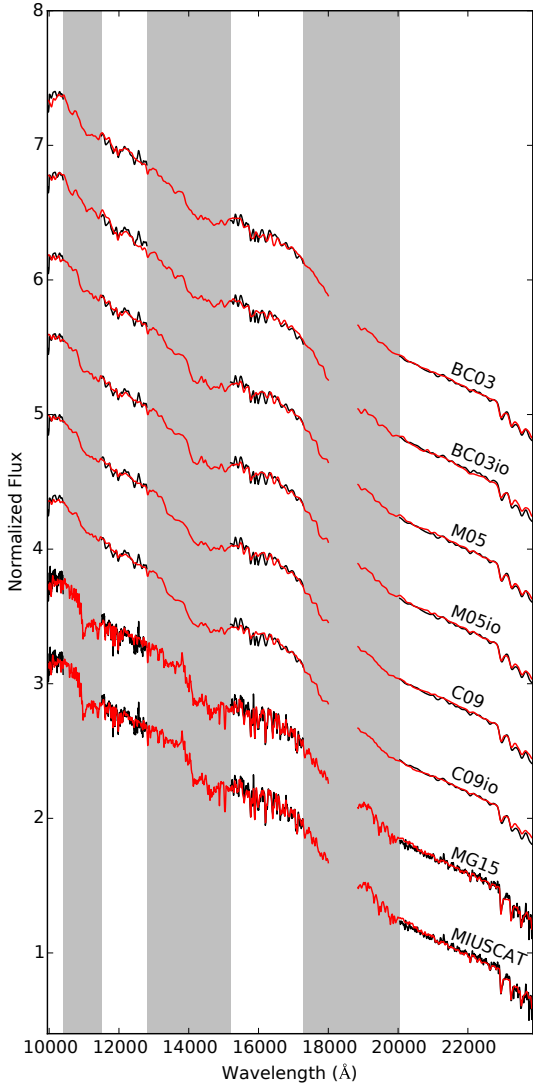


Figure 7. Same as Figure 4 but for NGC 6081

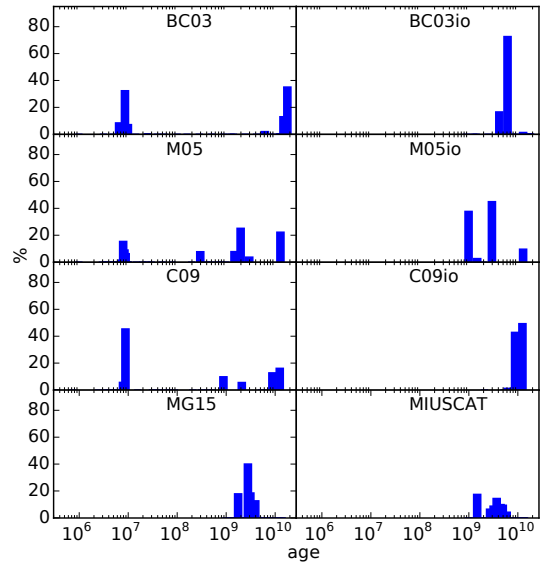
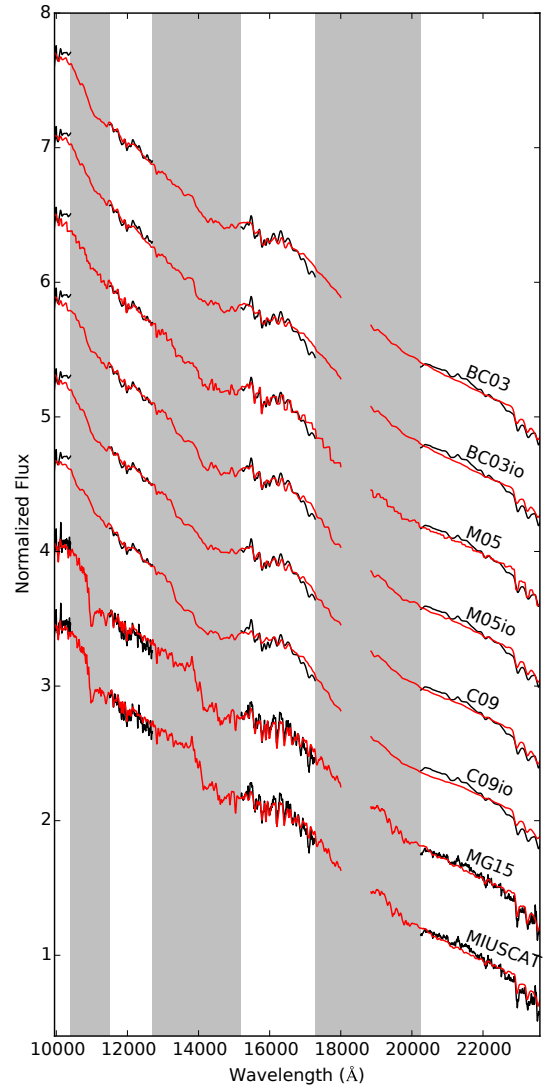


Figure 8. Same as Figure 4 but for NGC 6146

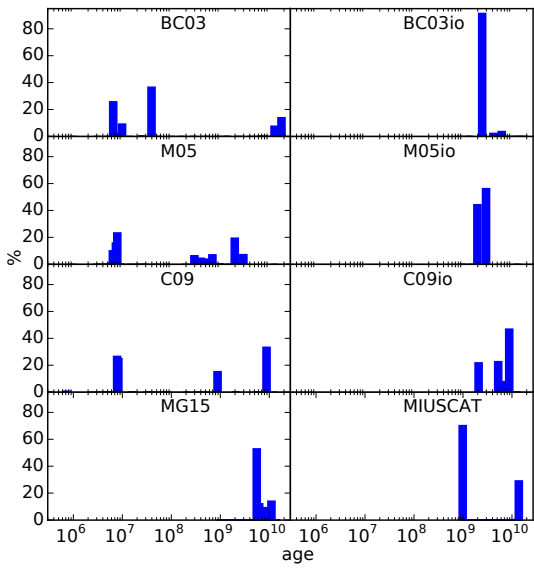
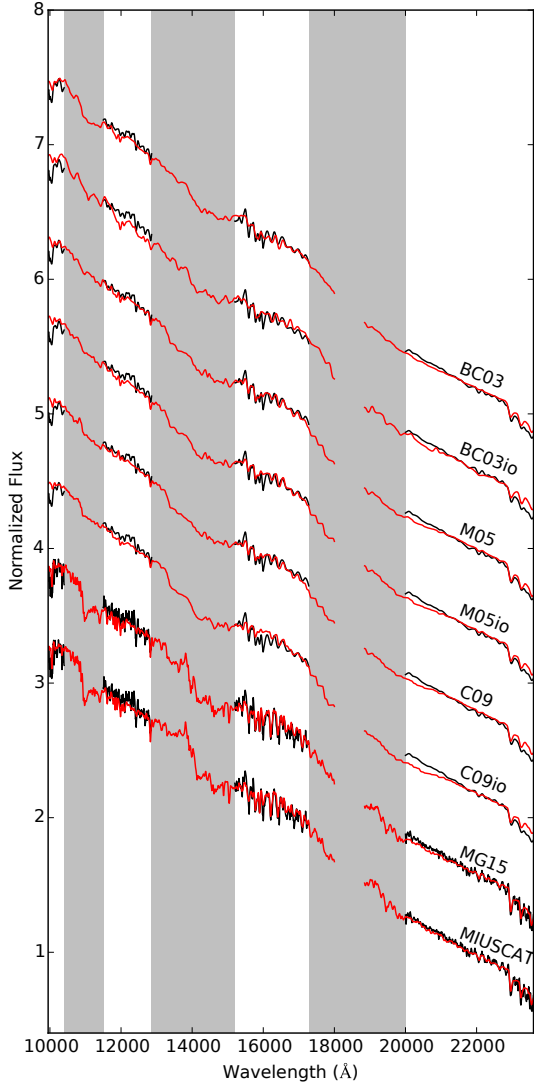


Figure 9. Same as Figure 4 but for NGC 6338

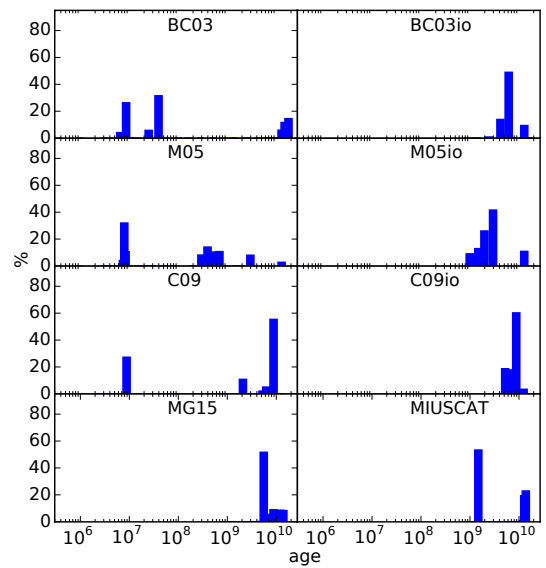
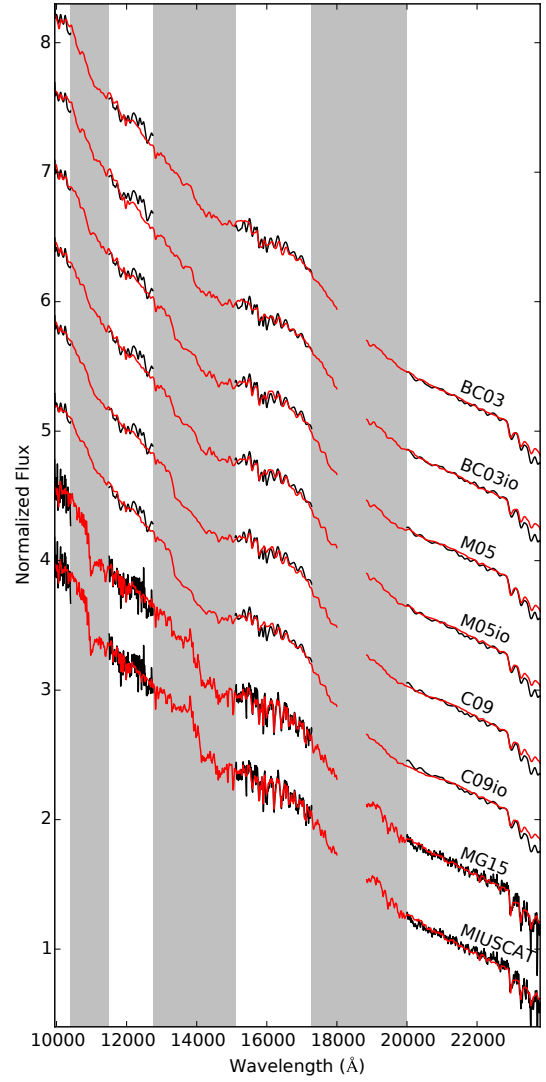


Figure 10. Same as Figure 4 but for UGC 08234

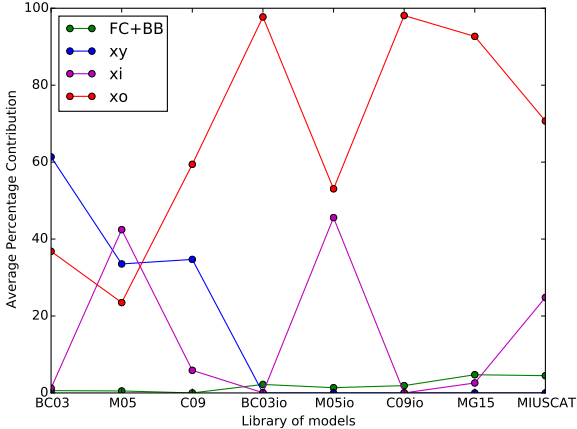


Figure 11. Average percentage contribution for each library of models. Young populations are displayed in blue, intermediate-aged populations in magenta and old stellar populations in red. In green, the summed contributions from featureless continuums and black bodies.

5.2 NIR models with high spectral resolution

For EPS models with high spectral resolution (MG15 and MIUSCAT), the above scenario improved considerably. For three objects (NGC 4636, NGC 5966 and NGC 6081), besides the small ($<10\%$) contribution from dust, only old SSPs were found using both libraries of models. For NGC 6146, both libraries predict a contribution of intermediate populations of $\sim 18\%$. For NGC 5905, the only spiral galaxy in our sample, a contribution of 31% from intermediate-age stars was obtained with MIUSCAT, but this same percentage was not detected when using MG15. Lastly, for UGC 08234, the fit with MG15 SSPs appear dominated by old populations. However, when MIUSCAT models are employed, the fits become dominated by intermediate-age stellar populations.

Note that it is not possible to fully test libraries with high spectral resolution, because MG15 and MIUSCAT are only composed of SSPs older than 1 Gyr. However, the results we obtained point toward an improvement when using libraries with high resolution. Also, the dust extinction values found with high spectral resolution libraries are much more consistent with literature results that showed that ETGs have very low amounts of dust.

5.3 Comparison with optical results

For the optical region, we also fit the data using the different libraries of models. Since MG15 models are only available in the NIR, we performed the synthesis using only BC03, M05, C09 and MIUSCAT libraries. Also, for a fair comparison between optical and NIR results, we performed the fits using the libraries without the young ages, *i.e.* BC03io, M05io and C09io. Figure 12 and Figure 13 present the optical synthesis results for the 6 galaxies with optical spectra. For each galaxy, we show the observed spectra in black and the model spectrum in red. On Figure 14 and Figure 15, we show the light fraction for each age in blue. The binned light and mass

contribution, along with the A_V , $\langle t \rangle_L$, $\langle Z \rangle_L$ and the A_{dev} for each galaxy are shown in Table 4.

In the optical synthesis, the different libraries of models produced results that are more similar among each other than those derived from the NIR. The only exception were the fits with M05 and M05io models, that also in the optical found a high fraction of intermediate populations. For the other libraries, in the optical region, the synthesis found a dominant contribution of old populations to the light of NGC 4636, NGC 5966, NGC 6081, NGC 6146 and NGC 6338 and a dominance of intermediate-age populations for UGC 08234. Using M05, on the other hand, the synthesis found similar results for all the objects, with small ($\lesssim 5\%$) contributions of young populations and higher fractions of intermediate age ($25\% \lesssim x_i \lesssim 55\%$) and old ($40\% \lesssim x_i \lesssim 75\%$) populations. It is worth mentioning that when using BC03 to fit the optical spectra, a larger contribution from young stellar populations is found compared to the other libraries. However, the dominant old population (or intermediate for UGC 08234) still remains the same found with the other libraries (see Table 4), while in the NIR spectral range, the dominant population contributing to the galaxy emission was different (see Table 3). Removing the SSPs with $t < 1$ Gyr from BC03 did not change the results.

For a proper comparison between optical and NIR results, we present in figs. 16 to 23 the values of x_y , x_i , x_o , A_V , $\langle t \rangle_L$ and $\langle Z \rangle_L$ found by STARLIGHT both for the optical and NIR ranges. The x axis displays the optical results and the y axis displays the NIR results found by STARLIGHT for the 8 different libraries of models used. For MG15 library, since it only has the NIR range of the spectra, we compared it to the optical results obtained with MIUSCAT. Over the 6 panels of each picture, we plotted a solid line, representing a perfect correlation between optical and NIR. Over the x_y , x_i and x_o panels, we also plotted two dashed lines showing the 10% error margin and two dotted lines showing the 30% error margin. Over the A_V panel, we plotted two dashed lines showing the 0.1 magnitude error margin and two dotted lines showing the 0.3 magnitude error margin. For the $\langle t \rangle_L$ and $\langle Z \rangle_L$ panels, since they are logarithmic scales, we did not display error margins.

From figs. 16 to 23, it is possible to see that libraries with low spectral resolution and with young populations usually disagrees in the optical and the NIR about the fractions of each stellar populations that contributes to the galaxy integrated light. It is clear that the fits using BC03, BC03io, C09 and C09io overestimate the amount of younger stellar populations in the NIR when compared to the fits in the optical. On the other hand, the fits with M05 and M05io are more self consistent when comparing optical and NIR results, where in both cases sizable amounts of intermediate age stars are found. All the tests with the lower spectral resolution models displayed a tendency to find extinctions ~ 1 magnitude higher when fitting the NIR spectral range, compared to optical one. Regarding the metallicity, fits with C09 find lower metallicities in the NIR compared to the optical, whereas BC03 and M05 fits using NIR or optical data converge to nearly the same metallicities.

When SSPs with $t \leq 1$ Gyr were removed from the libraries, the stellar populations found in the optical and NIR were much closer to each other. From the three libraries with low resolution and without young SSPs, M05io was the

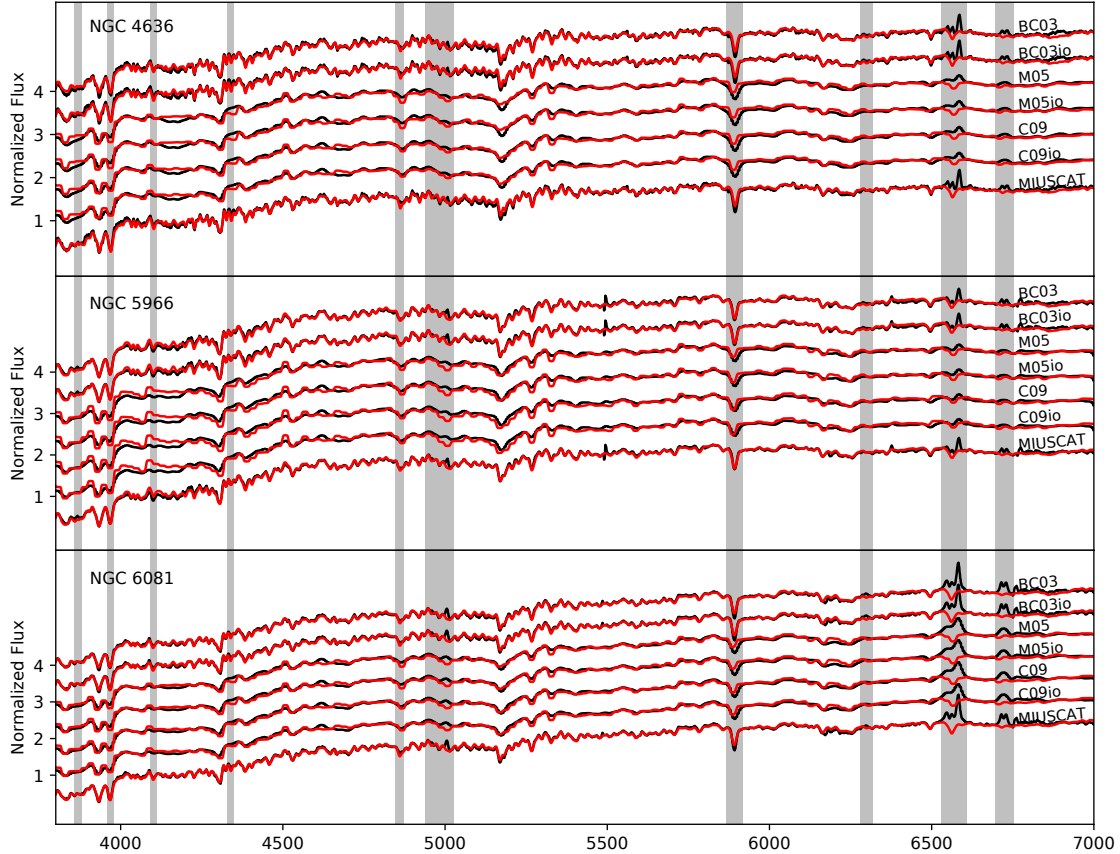


Figure 12. Optical fits for NGC 4636, NGC 5966 and NGC 6081. For each galaxy we present the observed (black) and modeled spectra (red) for the 4 libraries used.

one that found the most consistent results between the two wavelength ranges, with all the points in the xi and xo panels inside the 30% error margin. However, since the amounts of intermediate-age SSPs found with this library are close to $\sim 50\%$ and the sample is mainly composed of ETGs, these results suggest that both wavelength ranges tend equally to overestimate the amount of intermediate-age SSPs.

For BC03io, we found larger amounts of intermediate age stars in the optical than in the NIR, where only old SSPs contributed to the fits. For the tests with C09io, we found a dominant contribution from old SSPs in both spectral ranges. The only exception was UGC 08234, that a contribution of 85% of intermediate-age SSPs was required in the optical but only old SSPs were used in the NIR. When dealing with the reddening, these libraries also tend to overestimate the value of A_V by ~ 1 magnitude.

The high resolution models, on the other hand, perform considerably better, producing self consistent fits from NIR and optical fits. The reddening found with MG15 models is almost the same for the two wavelength ranges for the whole

sample, while MIUSCAT fits required an A_V 0.3mag larger for two objects. From the two last panels of figs. 22 and 23, it is possible to see that for both libraries, optical and NIR tend to find similar values of $\langle t \rangle_L$ and MG15 tends to find lower values of $\langle Z \rangle_L$ in the NIR when compared to the optical.

Unfortunately, there are no libraries of high resolution models that include SSPs younger than 1Gyr, meaning that the full scenario cannot be tested. However, our results suggest that high resolution models are essential to correctly disentangle the stellar population of a galaxy in the NIR, allowing in addition reliable reddening values. Otherwise, it is not possible to fit the absorptions and too much weight is given to the featureless continuum.

Baldwin et al. (2017) found that the impact of age variation in the near-infrared is largely dependent on the shape of the continuum. Our results show that the scenario is more complex, where the shape of the continuum is dependent on a combination of age and extinction, while the depth, shape and width of the absorption features are crucially shaped

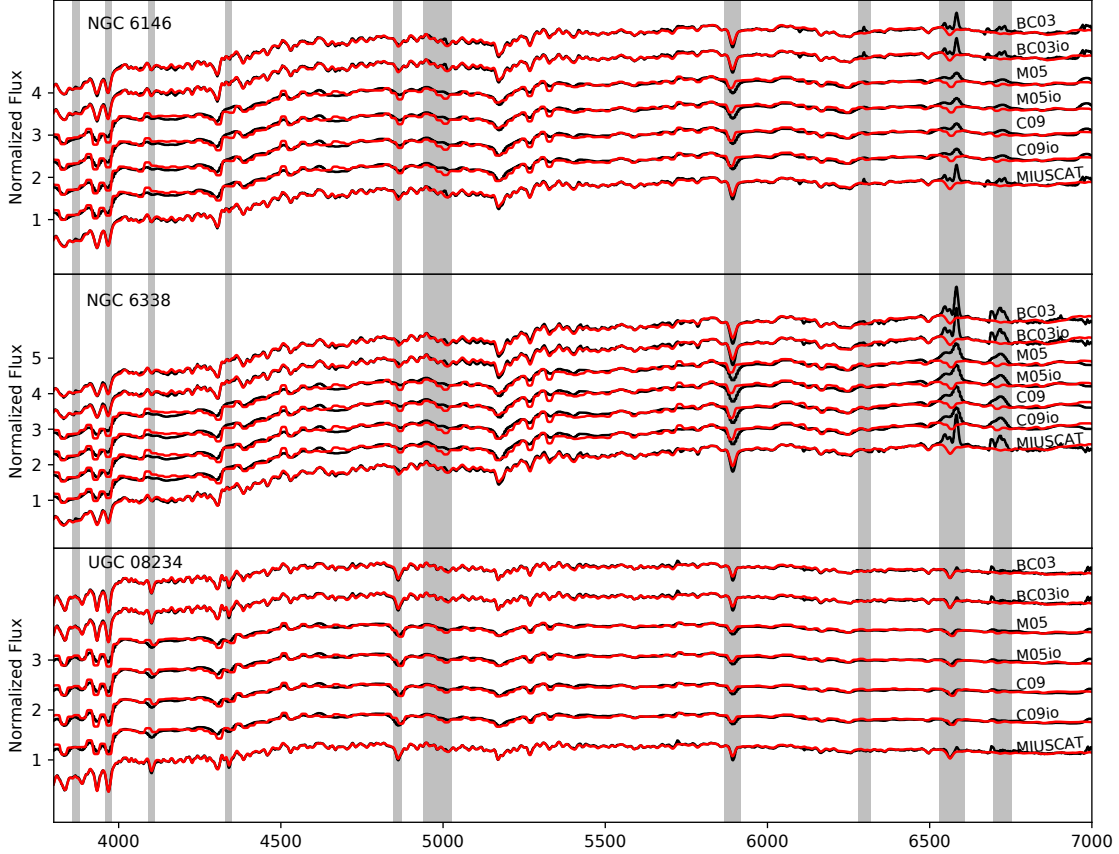


Figure 13. Same of Figure 12 but for NGC 6146, NGC 6338 and UGC 08234.

by the age of the population. For low resolution SSPs these features will be diluted. As a result, STARLIGHT will have more difficulties to differentiate among the individual SSPs. Therefore, we reinforce the need of adequate NIR stellar libraries for hotter stars, allowing thus the production of models with ages younger than 1 Gyr. This is specially important to properly fit the stellar content of active starforming galaxies.

5.4 Absorption Band Measurements

For comparison with future NIR SP studies, we computed the equivalent widths (W_λ) of the NIR absorption features measured with a python version of pacce code (Riffel & Borges Vale 2011). The values of W_λ are presented on Table 5. They were calculated based on the line limits and continuum bandpasses of Table 6. Mild correlations were found between CO16a and MgI, CO16b and SII, CO16c and NaI, CO16d and NaI, FeI and CaI, and the CO22 bands. Since the sample is small, these correlations should be seen with caution.

6 FINAL REMARKS

In this work we compared the stellar population of a sample of 6 ETGs and one spiral galaxy, both in the optical and NIR spectral ranges. We chose for the NIR 8 different bases of SSPs with different spectral resolutions and using different sets of isochrones to separately discuss their effects on the synthesis results. For 4 of the ETGs, we performed spectral synthesis in the optical using SDSS spectra and compared the results with those of the NIR. The approach followed here is based on the STARLIGHT code, which considers the whole observed spectrum, both the continuum and absorption features.

The main results can be summarized as follows: for spectral synthesis using bases with low spectral resolution, the results are more linked to the library of models used rather than to the object properties themselves. While BC03 models display a trend toward higher contributions of young populations, M05 usually finds more contributions from intermediate age populations whereas C09 tend to find higher contributions from old stellar populations. On all the cases,

Table 4. Results for the optical synthesis.

Library	xy	xi	xo	my	mi	mo	Av	$\langle t \rangle_L$	$\langle Z \rangle_L$	Adev
NGC 4636										
BC03	17.1	4.3	78.4	0.0	0.1	99.8	-0.01	9.51	0.02398	1.93
M05	2.8	55.6	41.4	0.0	7.3	92.6	0.40	9.31	0.03275	2.50
C09	0.0	2.4	97.5	—	—	—	0.25	9.86	0.01811	2.37
BC03io	0.0	33.7	66.2	0.0	1.2	98.8	0.02	9.82	0.02305	2.02
M05io	0.0	60.7	39.2	0.0	14.2	85.7	0.37	9.39	0.0296	2.59
C09io	0.0	5.4	94.5	—	—	—	0.25	9.86	0.01895	2.38
MIUSCATIR	0.0	22.6	77.3	—	—	—	0.28	9.88	0.02315	1.95
NGC 5966										
BC03	0.0	11.0	88.4	0.0	1.0	98.9	-0.01	10.11	0.02526	1.84
M05	0.0	26.8	73.2	0.0	2.5	97.4	0.26	9.77	0.02563	3.61
C09	0.0	0.0	100.0	—	—	—	0.16	9.90	0.02232	3.89
BC03io	0.0	15.1	84.8	0.0	1.4	98.5	-0.00	10.08	0.0265	1.83
M05io	0.0	40.5	59.5	0.0	9.9	90.0	0.23	9.73	0.02708	3.65
C09io	0.0	0.0	100.0	—	—	—	0.16	9.88	0.02289	3.89
MIUSCATIR	0.0	0.0	100.0	—	—	—	0.18	10.09	0.02663	1.74
NGC 6081										
BC03	5.0	23.9	71.0	0.0	1.1	98.8	0.69	9.75	0.01817	1.60
M05	0.0	49.8	50.1	0.0	6.5	93.4	0.91	9.53	0.02232	2.48
C09	0.0	0.0	100.0	—	—	—	0.85	9.87	0.01503	2.60
BC03io	0.0	34.6	65.3	0.0	1.6	98.3	0.71	9.82	0.01778	1.69
M05io	0.0	47.7	52.2	0.0	6.1	93.8	0.88	9.59	0.0181	2.51
C09io	0.0	0.0	100.0	—	—	—	0.84	9.92	0.01447	2.59
MIUSCATIR	0.0	16.7	83.2	—	—	—	0.92	9.83	0.02177	1.49
NGC 6146										
BC03	6.6	9.6	83.0	0.0	0.3	99.6	-0.03	9.84	0.0213	1.29
M05	0.0	38.6	61.4	0.0	4.4	95.5	0.28	9.60	0.02732	2.65
C09	0.0	0.0	100.0	—	—	—	0.16	9.89	0.02022	2.72
BC03io	0.0	13.3	86.6	0.0	0.5	99.5	-0.02	10.04	0.01982	1.33
M05io	0.0	33.3	66.6	0.0	4.5	95.4	0.26	9.71	0.02072	2.70
C09io	0.0	0.0	100.0	—	—	—	0.16	9.88	0.02289	3.89
MIUSCATIR	0.0	13.0	86.9	—	—	—	0.22	9.91	0.02246	1.13
NGC 6338										
BC03	1.3	1.0	94.0	0.0	0.0	99.9	0.33	10.16	0.02569	1.77
M05	0.0	25.2	74.8	0.0	2.3	97.6	0.67	9.79	0.02561	3.17
C09	0.0	0.0	100.0	—	—	—	0.53	10.05	0.01783	3.36
BC03io	0.0	0.9	99.0	0.0	0.0	99.9	0.33	10.22	0.02434	1.78
M05io	0.0	21.5	78.4	0.0	2.0	97.9	0.65	9.87	0.02038	3.22
C09io	0.0	0.0	100.0	—	—	—	0.53	10.03	0.01938	3.34
MIUSCATIR	0.0	3.7	96.2	—	—	—	0.59	10.10	0.02628	1.63
UGC 08234										
BC03	0.0	86.5	13.4	0.0	26.2	73.7	-0.07	9.15	0.04017	1.18
M05	0.0	40.0	60.0	0.0	8.5	91.4	0.03	9.28	0.02446	2.12
C09	0.0	65.5	34.4	—	—	—	0.23	9.28	0.02118	2.32
BC03io	0.0	85.0	14.9	0.0	25.9	74.1	-0.07	9.21	0.0368	1.18
M05io	0.0	42.7	57.2	0.0	14.0	85.9	-0.05	9.34	0.01896	2.20
C09io	0.0	61.5	38.4	—	—	—	0.21	9.29	0.01998	2.32
MIUSCATIR	0.0	67.1	32.8	—	—	—	0.07	9.40	0.02134	1.00

Table 5. Equivalent widths for the NIR absorption bands measured in Å.

Galaxy/Line	CO16a	CO16b	SiI	CO16c	CO16d	FeI	MgI	NaI	CaI	CO22a	CO22b	CO22c
Average Error	0.10	0.12	0.13	0.32	0.22	0.12	0.8	0.21	0.21	0.86	1.24	1.58
NGC4636	2.06	3.08	1.97	6.41	4.71	0.42	2.47	4.55	2.86	16.42	18.81	18.01
NGC5905	1.69	3.69	3.03	7.61	5.03	0.47	2.03	5.79	4.08	17.50	6.78	8.94
NGC5966	1.74	4.29	3.72	7.17	3.89	0.37	2.41	4.68	2.23	7.79	4.73	6.68
NGC6081	0.23	3.18	2.77	6.53	3.40	0.53	1.95	3.68	3.26	19.77	24.23	27.59
NGC6146	2.38	4.23	4.07	5.89	3.72	0.39	2.55	2.50	1.65	34.72	46.77	50.05
NGC6338	2.31	3.13	2.90	5.53	4.34	0.47	2.10	3.57	3.76	13.79	13.60	8.64
UGC08234	1.29	3.36	3.36	5.24	3.91	—	1.82	2.20	3.69	17.77	25.97	35.33

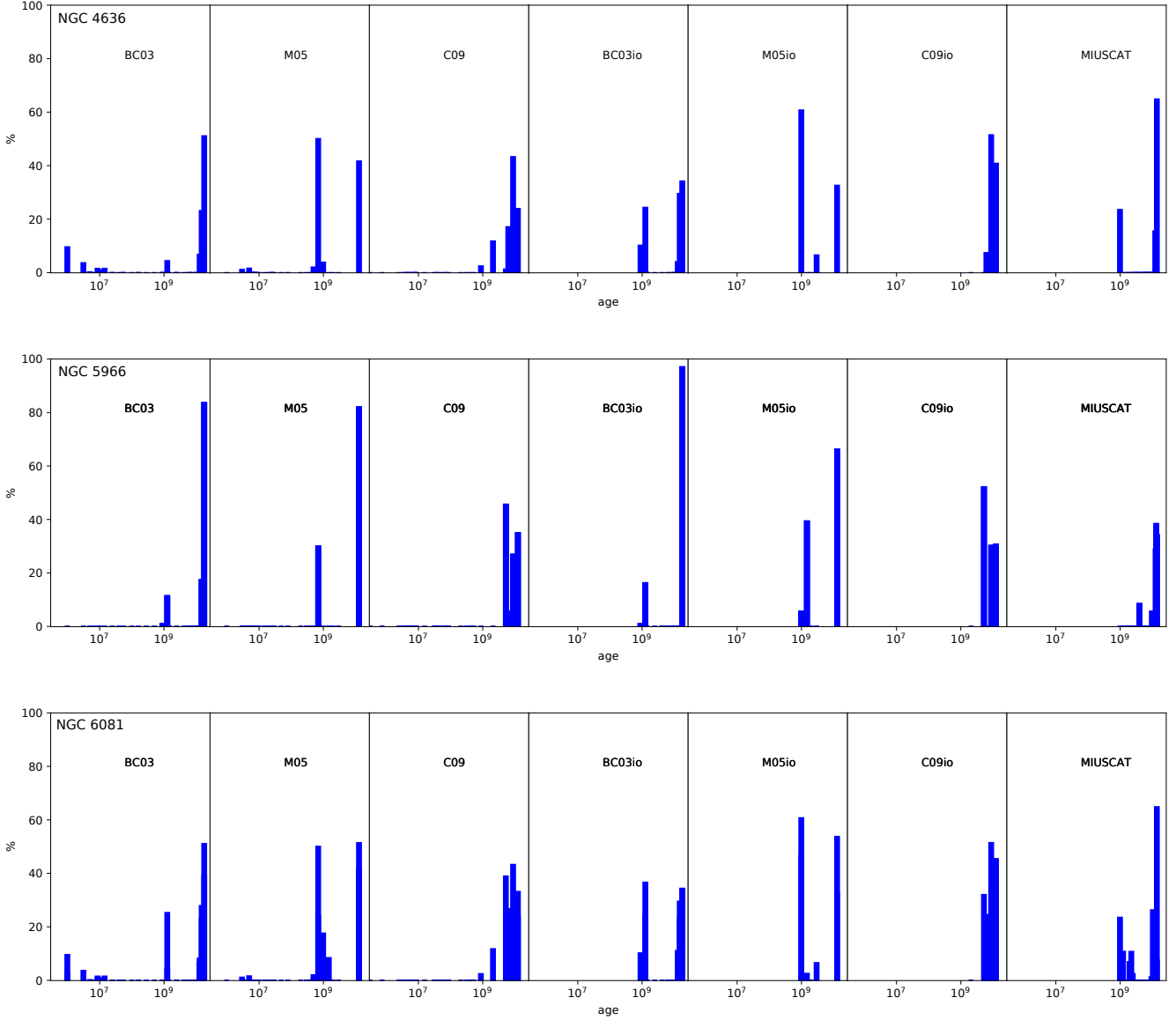


Figure 14. Optical star formation histories for NGC 4636, NGC 5966 and NGC 6081, metallicities summed.

the values of A_{dev} are compatible, meaning that none of these bases offer a more reliable result. When using bases with high spectral resolution, MG15 and MIUSCAT produced more consistent results if compared to low spectral resolution libraries. Out of the 7 galaxies, the two libraries fitted consistent results for six of them.

The optical synthesis for the elliptical galaxies revealed a dominance of old stellar populations. The only exception was M05 library, which still found a high fraction of intermediate age populations. This may indicate that the TP-AGB treatment plays an important role, even in the optical region.

When comparing optical and NIR results, we found that NIR fits using low spectral resolution libraries tend to overestimate the amount of young SSPs and the reddening. The only exception were the M05 models, which produced self con-

sistent fits, but predicted sizable amounts of intermediate age stars for the galaxies. For libraries with high spectral resolution, since they do not include young SSPs, this scenario cannot be fully tested. However, the reddening found was compatible with literature. Also, high spectral resolution libraries produced results much more consistent if compared to models with low spectral resolution.

We tabulated the equivalent widths (W_{λ}) of the NIR absorption features and the optical emission line fluxes to be used in future studies. Lastly, from the emission line ratios, we classified, for the first time in the literature, NGC 6081 and NGC 6338 as LINERs.

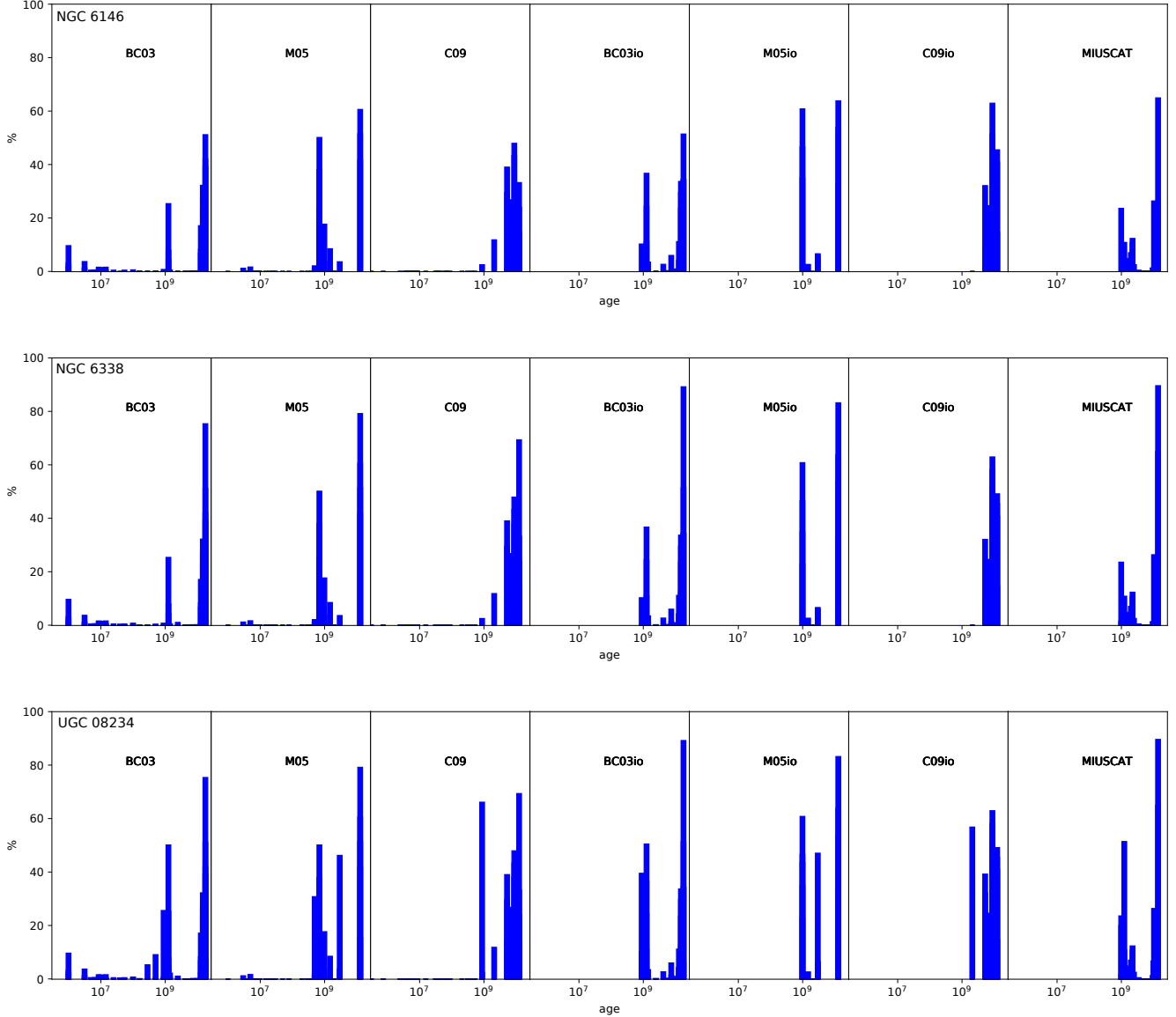


Figure 15. Same as Figure 14 but for NGC 6146, NGC 6338 and UGC 08234.

ACKNOWLEDGEMENTS

LGDH thanks CAPES and CNPq. RR thanks CNPq and FAPERGS for partial funding this project. ARA thanks CNPq for partial support to this work. LPM thanks CNPq and FAPESP for partial funding of this project. CK acknowledges support through the research project AYA2017-79724-C4-4-P from the Spanish PNAYA. This research made use of the NASA/IPAC Extragalactic Database (NED), which is operated by the Jet Propulsion Laboratory, California Institute of Technology, under contract with the National Aeronautics and Space Administration. This study uses data provided by the Calar Alto Legacy Integral Field Area (CALIFA) survey (<http://califa.caha.es/>). Based on observations collected at the Centro Astronómico Hispano Alemán (CAHA) at Calar Alto, operated jointly by the Max-

Planck-Institut für Astronomie and the Instituto de Astrofísica de Andalucía (CSIC). We thank the referee Reynier Peletier for carefully reading our paper and for giving such constructive comments which substantially helped improving the quality of the paper.

REFERENCES

- Baldwin J. A., Phillips M. M., Terlevich R., 1981, *PASP*, **93**, 5
 Baldwin C. M., McDermid R. M., Kuntschner H., Maraston C., Conroy C., 2017, preprint, ([arXiv:1709.09300](https://arxiv.org/abs/1709.09300))
 Bamford S. P., Rojas A. L., Nichol R. C., Miller C. J., Wasserman L., Genovese C. R., Freeman P. E., 2008, *MNRAS*, **391**, 607
 Bruzual G., Charlot S., 2003, *MNRAS*, **344**, 1000
 Caccianiga A., Marchã M. J., Antón S., Mack K.-H., Neeser M. J., 2002, *MNRAS*, **329**, 877

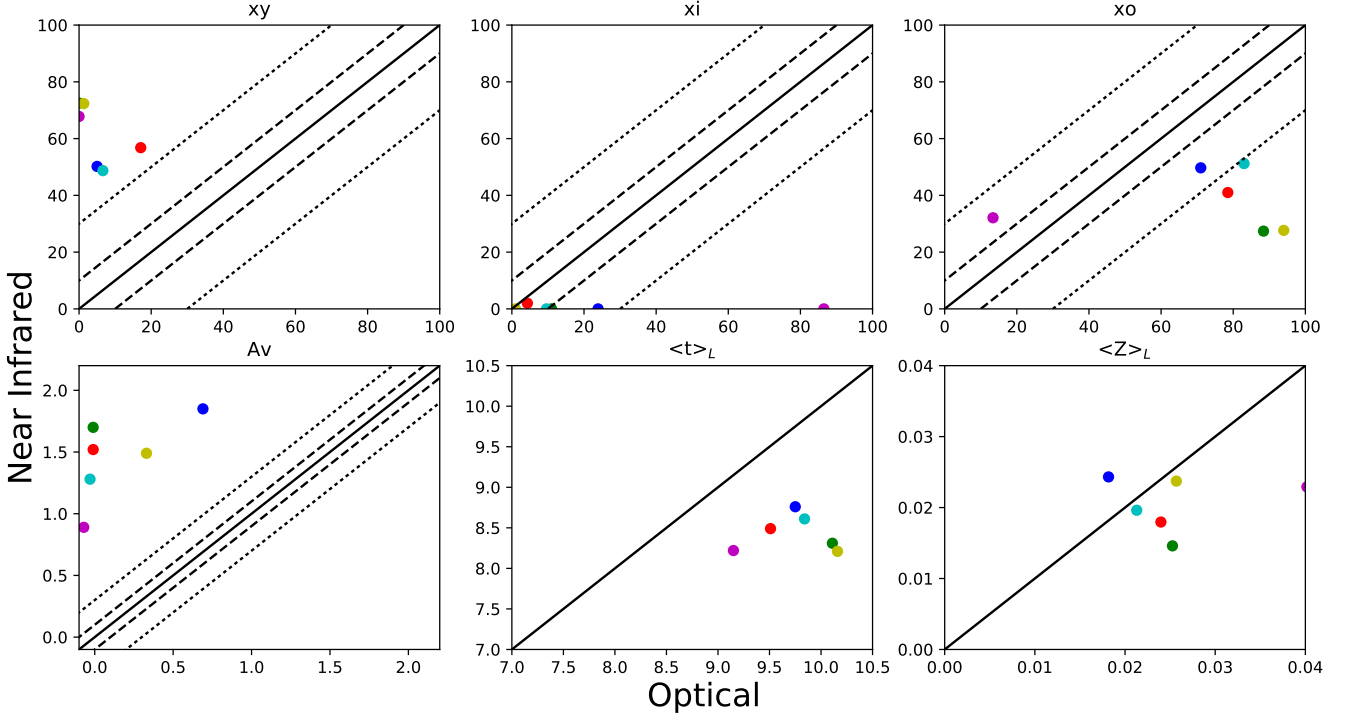


Figure 16. Comparison between optical and NIR results found using BC03 library of models. In the upper panels, we present from left to right the xy , xi and xo results. In the bottom panels, we show the A_V , $\langle t \rangle_L$ and $\langle Z \rangle_L$ results. Over all panels, we plotted a solid line, representing a perfect correlation between optical and NIR. Also, we plotted dashed and dotted lines representing error margins of 10 and 30% in the xy , xi and xo panel and error margins of 0.1 and 0.3 magnitudes in the A_V panel. Each galaxy was plotted in a different color: NGC 4636 - red, NGC 5966 - green, NGC 6081 - blue, NGC 6146 - cyan, NGC 6338 - yellow, UGC 08234 - magenta.

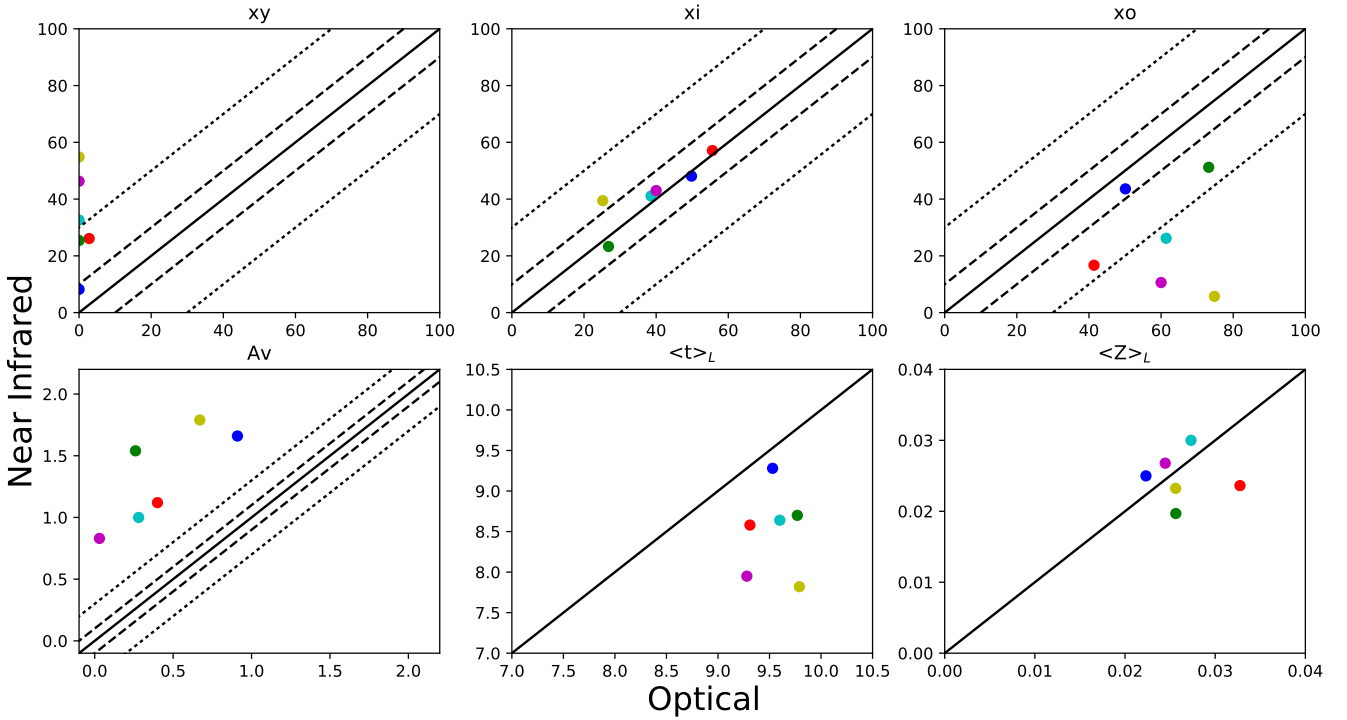


Figure 17. Same of Figure 16, but for M05 library of models.

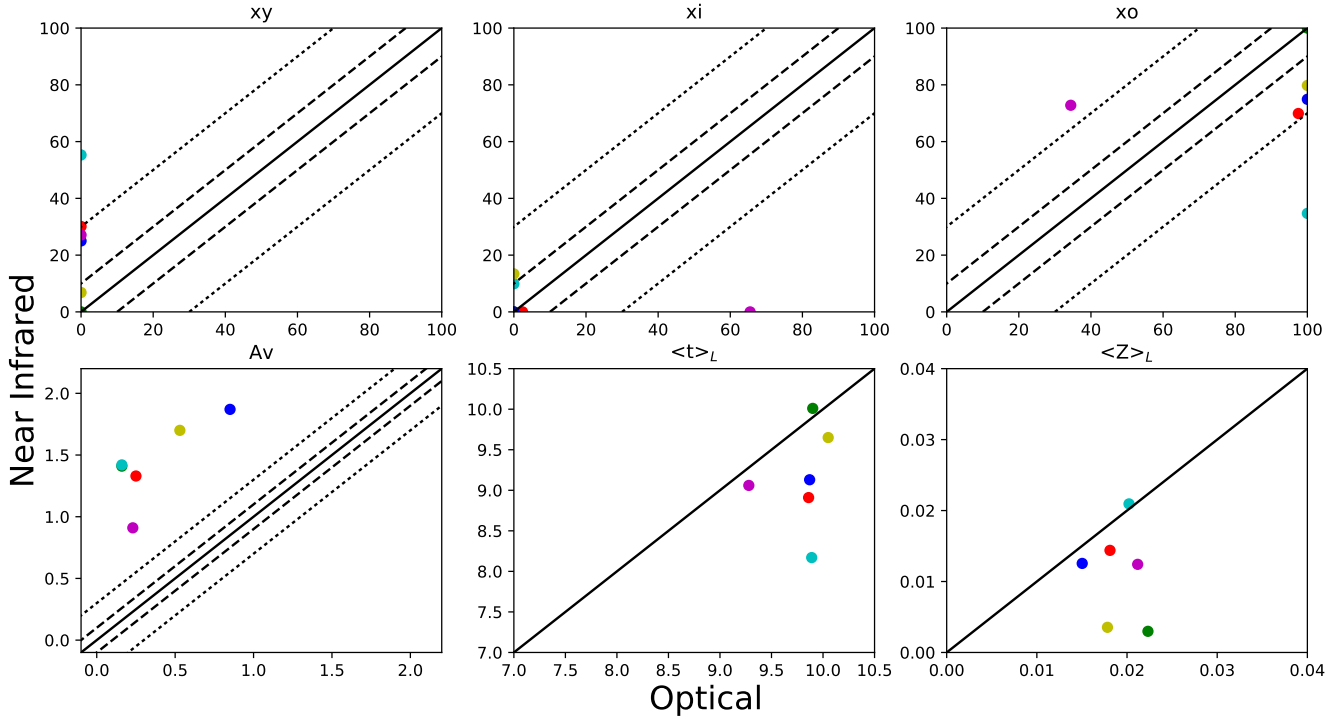


Figure 18. Same of Figure 16, but for C09 library of models.

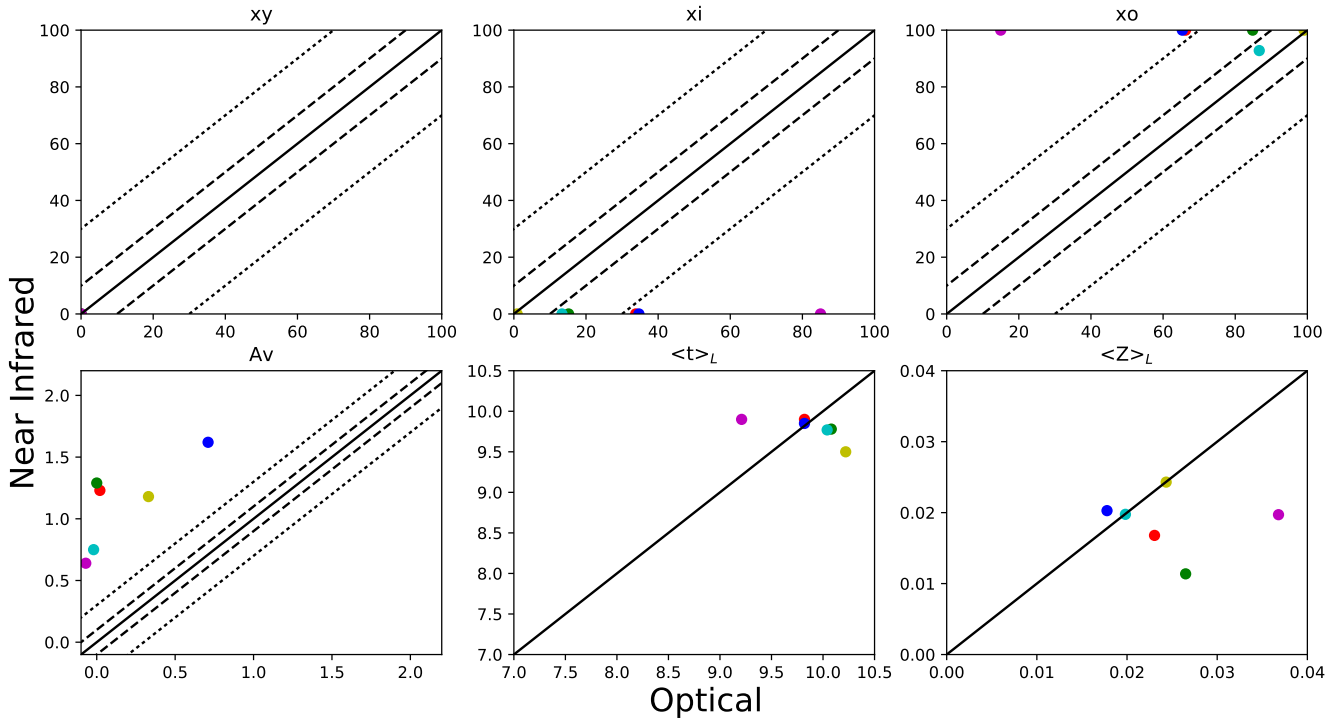


Figure 19. Same of Figure 16, but for BC03io library of models.

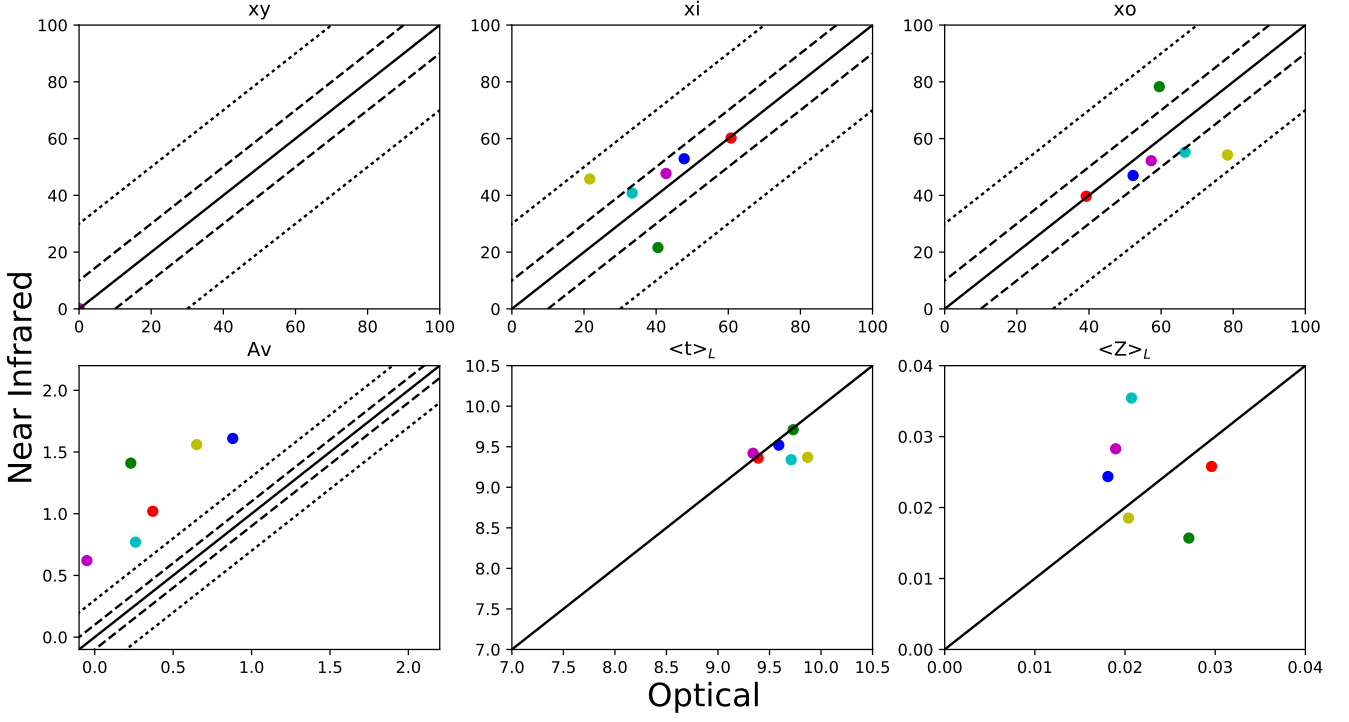


Figure 20. Same of Figure 16, but for M05io library of models.

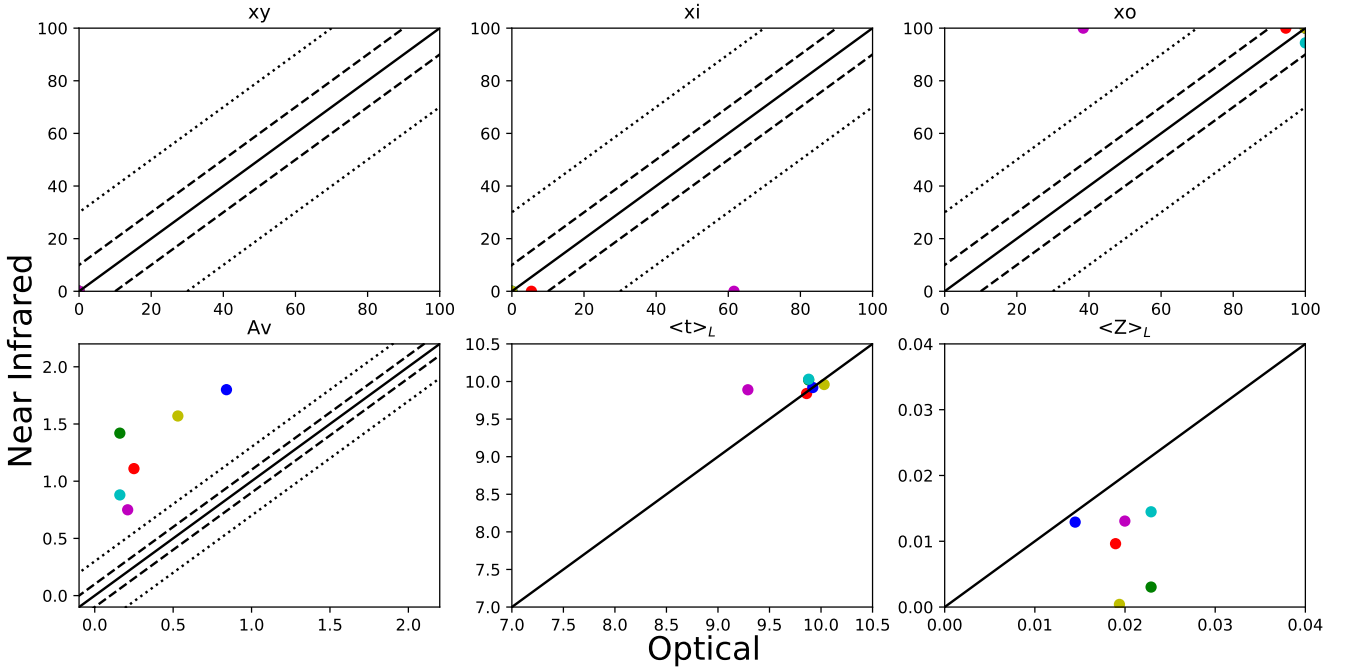


Figure 21. Same of Figure 16, but for C09io library of models.

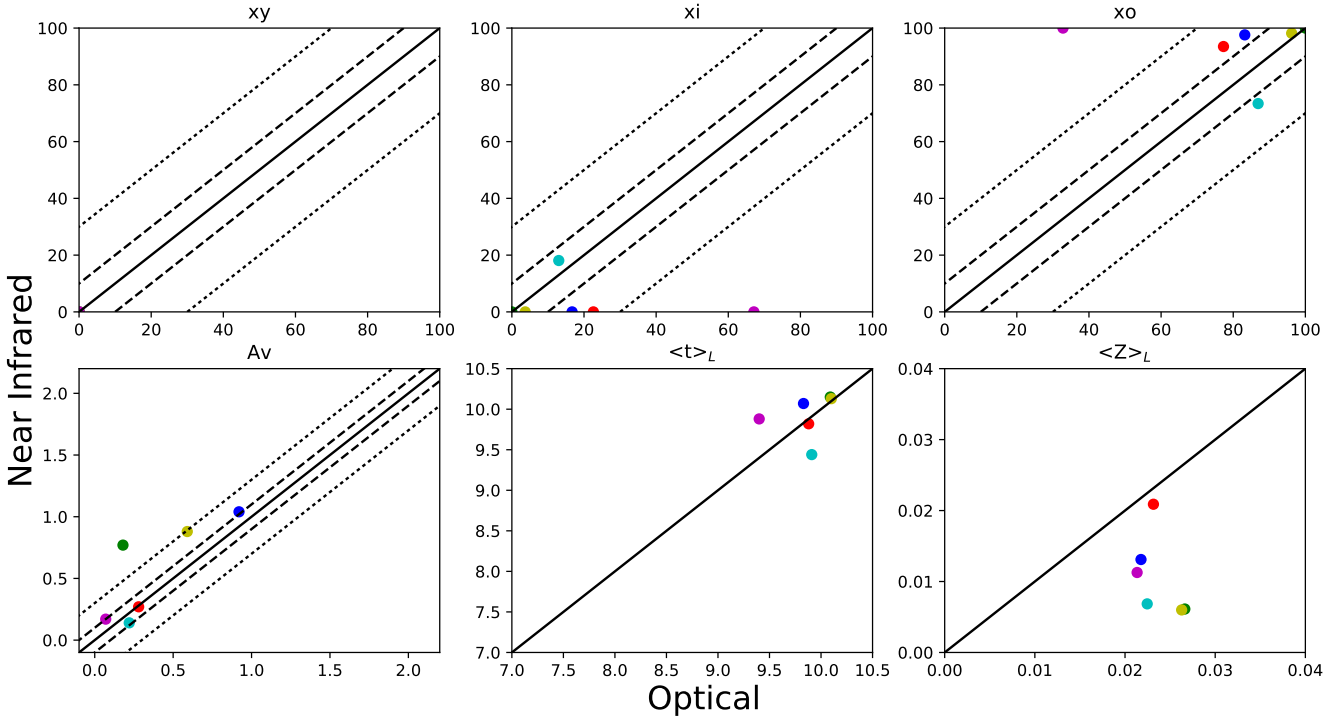


Figure 22. Same of Figure 16, but for MG15 library of models.

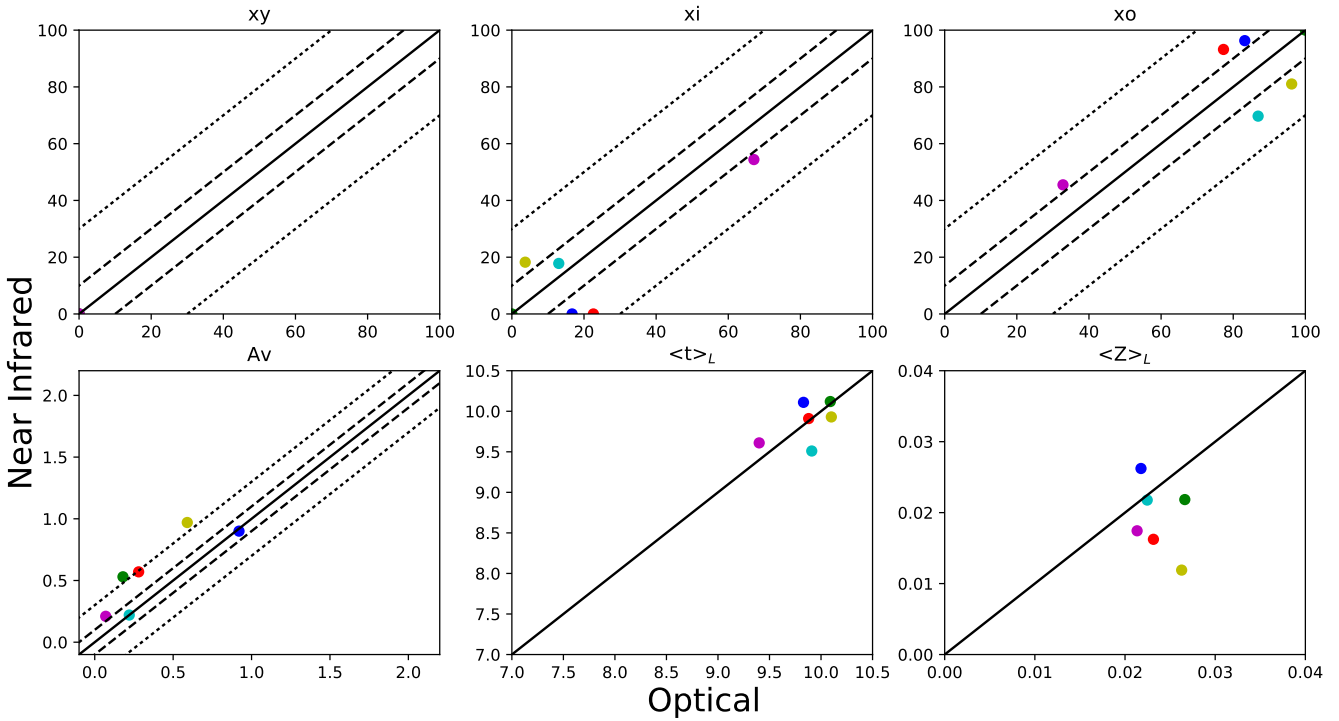


Figure 23. Same of Figure 16, but for MIUSCAT library of models.

Table 6. Line limits and continuum bandpasses.

Centre (Å)	Main Absorber	line limits (Å)	continuum bandpass (Å)
15587	CO	15555-15620	15110-15170, 15390-15410,16270-16310,16570-16580
15772	CO	15735-15810	15110-15170, 15390-15410,16270-16310,16570-16580
15890	Sir	15850-15930	15110-15170, 15390-15410,16270-16310,16570-16580
16215	CO	16145-16285	15110-15170, 15390-15410,16270-16310,16570-16580
16385	CO	16340-16430	15110-15170, 15390-15410,16270-16310,16570-16580
17054	FeI	17025-17083	16970-17083, 17140-17200
17106	MgI	17083-17130	16970-17083, 17140-17200
22025	NaI	21950-22100	21700-21930,22150-22200
22620	CaI	22570-22670	22450-22550,22680-22730
23015	CO	22870-23160	22690-22790, 23655-23680,23890-23920
23290	CO	23160-23420	22690-22790, 23655-23680,23890-23920
23535	CO	23420-23650	22690-22790, 23655-23680,23890-23920

Table Notes: The NIR indexes are based on Riffel et al. (2008, 2009, 2011, 2015).

- Capozzi D., Maraston C., Daddi E., Renzini A., Strazzullo V., Gobat R., 2016, *MNRAS*, **456**, 790
- Cardelli J. A., Clayton G. C., Mathis J. S., 1989, *ApJ*, **345**, 245
- Cassisi S., degl'Innocenti S., Salaris M., 1997a, *MNRAS*, **290**, 515
- Cassisi S., Castellani M., Castellani V., 1997b, *A&A*, **317**, 108
- Chen X. Y., Liang Y. C., Hammer F., Prugniel P., Zhong G. H., Rodrigues M., Zhao Y. H., Flores H., 2010, *A&A*, **515**, A101
- Cid Fernandes R., Gu Q., Melnick J., Terlevich E., Terlevich R., Kunth D., Rodrigues Lacerda R., Joguet B., 2004, *MNRAS*, **355**, 273
- Cid Fernandes R., Mateus A., Sodré L., Stasińska G., Gomes J. M., 2005, *MNRAS*, **358**, 363
- Conroy C., 2013, *ARA&A*, **51**, 393
- Conroy C., Gunn J. E., 2010, *ApJ*, **712**, 833
- Conroy C., Gunn J. E., White M., 2009, *ApJ*, **699**, 486
- Cushing M. C., Vacca W. D., Rayner J. T., 2004, *PASP*, **116**, 362
- Cushing M. C., Rayner J. T., Vacca W. D., 2005, *ApJ*, **623**, 1115
- Dametto N. Z., Riffel R., Pastoriza M. G., Rodríguez-Ardila A., Hernandez-Jimenez J. A., Carvalho E. A., 2014, *MNRAS*, **443**, 1754
- Dressel L. L., Condon J. J., 1978, *ApJS*, **36**, 53
- Forman W., Jones C., Tucker W., 1985, *ApJ*, **293**, 102
- Gomes J. M., et al., 2016, *A&A*, **588**, A68
- Höfner S., Loidl R., Aringer B., Jørgensen U. G., Hron J., 2000, in Salama A., Kessler M. F., Leech K., Schulz B., eds, *ESA Special Publication Vol. 456, ISO Beyond the Peaks: The 2nd ISO Workshop on Analytical Spectroscopy*. p. 299
- Jones C., Forman W., Vikhlinin A., Markevitch M., David L., Warmflash A., Murray S., Nulsen P. E. J., 2002, *ApJ*, **567**, L115
- Kehrig C., et al., 2012, *A&A*, **540**, A11
- Kriek M., et al., 2010, *ApJ*, **722**, L64
- Kroupa P., 2001, *MNRAS*, **322**, 231
- Lançon A., Mouhcine M., 2002, *A&A*, **393**, 167
- Le Borgne J.-F., et al., 2003, *A&A*, **402**, 433
- Lejeune T., Cuisinier F., Buser R., 1997, *A&AS*, **125**
- Lejeune T., Cuisinier F., Buser R., 1998, *A&AS*, **130**, 65
- Maraston C., 2005, *MNRAS*, **362**, 799
- Maraston C., Strömbäck G., 2011, *MNRAS*, **418**, 2785
- Marigo P., Girardi L., Bressan A., Groenewegen M. A. T., Silva L., Granato G. L., 2008, *A&A*, **482**, 883
- Martel A. R., et al., 2004, *AJ*, **128**, 2758
- Martins L. P., Lanfranchi G., Gonçalves D. R., Magrini L., Teodorescu A. M., Quireza C., 2012, *MNRAS*, **419**, 3159
- Martins L. P., Rodríguez-Ardila A., Diniz S., Gruenwald R., de Souza R., 2013, *MNRAS*, **431**, 1823
- Meneses-Goytia S., Peletier R. F., Trager S. C., Vazdekis A., 2015, *A&A*, **582**, A97
- Nilson P., 1973, Uppsala general catalogue of galaxies
- Noël N. E. D., Greggio L., Renzini A., Carollo C. M., Maraston C., 2013, *ApJ*, **772**, 58
- Padilla N. D., Strauss M. A., 2008, *MNRAS*, **388**, 1321
- Pandge M. B., Vagshette N. D., David L. P., Patil M. K., 2012, *MNRAS*, **421**, 808
- Pietrinferni A., Cassisi S., Salaris M., Castelli F., 2004, *ApJ*, **612**, 168
- Raichur H., Das M., Herrero A. A., Shastri P., Kantharia N. G., 2015, *Ap&SS*, **357**, 32
- Rayner J. T., Cushing M. C., Vacca W. D., 2009, *ApJS*, **185**, 289
- Rickes M. G., Pastoriza M. G., Bonatto C., 2009, *A&A*, **505**, 73
- Riffel R., Borges Vale T., 2011, *Ap&SS*, **334**, 351
- Riffel R., Pastoriza M. G., Rodríguez-Ardila A., Maraston C., 2007, *ApJ*, **659**, L103
- Riffel R., Pastoriza M. G., Rodríguez-Ardila A., Maraston C., 2008, *MNRAS*, **388**, 803
- Riffel R., Pastoriza M. G., Rodríguez-Ardila A., Bonatto C., 2009, *MNRAS*, **400**, 273
- Riffel R., Riffel R. A., Ferrari F., Storchi-Bergmann T., 2011, *MNRAS*, **416**, 493
- Riffel R., et al., 2015, *MNRAS*, **450**, 3069
- Röck B., Vazdekis A., Ricciardelli E., Peletier R. F., Knapen J. H., Falcón-Barroso J., 2016, *A&A*, **589**, A73
- Salpeter E. E., 1955, *ApJ*, **121**, 161
- Sánchez S. F., et al., 2012, *A&A*, **538**, A8
- Sánchez S. F., et al., 2016, *A&A*, **594**, A36
- Schaller G., Schaerer D., Meynet G., Maeder A., 1992, *A&AS*, **96**, 269
- Schmidt A. A., Copetti M. V. F., Alloin D., Jablonka P., 1991, *MNRAS*, **249**, 766
- Stanger V. J., Warwick R. S., 1986, *MNRAS*, **220**, 363
- Vacca W. D., Cushing M. C., Rayner J. T., 2004, *PASP*, **116**, 352
- Véron-Cetty M.-P., Véron P., 2006, *A&A*, **455**, 773
- Walcher C. J., et al., 2014, *A&A*, **569**, A1
- Westera P., Lejeune T., Buser R., Cuisinier F., Bruzual G., 2002, *A&A*, **381**, 524
- Wilson J. C., et al., 2004, in Moorwood A. F. M., Iye M., eds, *Proc. SPIE Vol. 5492, Ground-based Instrumentation for Astronomy*. pp 1295–1305, doi:10.1117/12.550925
- Worthey G., 1994, *ApJS*, **95**, 107
- Wrobel J. M., 1984, *ApJ*, **284**, 531
- Zibetti S., Gallazzi A., Charlot S., Pierini D., Pasquali A., 2013, *MNRAS*, **428**, 1479

de Vaucouleurs G., de Vaucouleurs A., Corwin Jr. H. G., Buta R. J., Paturel G., Fouqué P., 1991, Third Reference Catalogue of Bright Galaxies. Volume I: Explanations and references. Volume II: Data for galaxies between 0^h and 12^h . Volume III: Data for galaxies between 12^h and 24^h .

APPENDIX A: INDIVIDUAL DESCRIPTION OF THE SAMPLE

A1 NGC 4636

NGC 4636 is a giant elliptical galaxy with LINER emission. Is one of the nearest and more X-ray luminous ellipticals, with L_X 2×10^{41} ergs/s (Jones et al. 2002). It is surrounded by an extended corona of hot gas (Forman et al. 1985), and has an asymmetric gas distribution, probably the result of irregular flows (Stanger & Warwick 1986).

A2 NGC 5905

This galaxy is one of a few that did not have a previously evidence of an AGN but that had X-ray eruptions observed, what happened in 1991 and 1992 with Chandra telescope. Later, X-ray flux started to decrease in a rate consistent with the expected for a Tidal Disruption Event (TDE). Recent observations showed that the infrared flux is dominated by star formation, what suggests that the radio emission is caused by circumnuclear star formation. Besides, no radio emission consistent with the TDE event was detected (Raichur et al. 2015). Among the galaxies of our sample, it is the only that has clearly visible NIR emission lines an the only non-ETG.

A3 NGC 5966

NGC 5966 is an elliptical galaxy with a faint bar-like feature centered at the nucleus. Stars and gas are decoupled, with the gas showing an elongated emission feature, in such a way that an ionization cone or a decoupled rotational disk are two possible interpretations (Kehrig et al. 2012). According to these authors, the diagnostic diagrams indicate the presence of a LINER nucleus and a LINER-like gas emission extending ~ 5 kpc outward from the nucleus, also LINER-like. The presence of a nuclear ionizing source seems to be required to shape the elongated gas emission feature in the ionization cone" scenario, although ionization by pAGB stars cannot be ruled out. On the other hand, Gomes et al. (2016) classified this object as type i ETG, also reporting that the absence of ongoing star formation throughout the galaxy lends support to the idea that its gas outflow is powered by an AGN hosted in its LINER nucleus. According to Gomes et al. (2016), a Type i ETG is a system with a nearly constant $EW(H\alpha)$ in their extranuclear component, compatible with the hypothesis of photoionization by pAGB as the main driver of extended warm interstellar medium (WIM) emission.

A4 NGC 6081

It is a galaxy with radio emission (Dressel & Condon 1978). Also, Gomes et al. (2016) classified it as a type i ETG, reporting that sources other than pAGB stars dominate in less

Table B1. NIR emission line fluxes measured for NGC 5905.

Line	Flux ($\times 10^{-15}$ ergs/s/cm 2)	FWHM (km/s)
[FeII] $\lambda 12570$	9.33	806
Pa β	6.72	315
H $_2$ $\lambda 21218$	2.68	385
Bry	3.5	462

than 7% of the area of the galaxy. Its SDSS spectra is dominated by stellar population, with strong absorption bands and [OIII], [NI], $H\alpha$ and [SII] typical of LINERs. It's APO spectrum shows a stellar continuum dominated source with strong CO bands and absence of emission lines.

A5 NGC 6146

NGC 6146 is an elliptical galaxy with a radio jet (Wrobel 1984). Caccianiga et al. (2002) reported the detection of CaII H and K, G, Mg Ib and Na Id absorption bands and a weak $H\alpha$ emission line. Gomes et al. (2016) classified this galaxy as type i ETG, also reporting that the absence of star formation and the suggestion of an outflow are compatible with the idea of a low luminosity AGN powering the nucleus. Its APO spectra shows a stellar continuum dominated source with strong CO bands and absence of emission lines.

A6 NGC 6338

This galaxy is the brightest on Draco constellation. It possesses diffuse and ionized gas and dust filaments on kiloparsec scales (Martel et al. 2004). X-ray observations indicate two or possibly three emission cavities of ellipsoidal shape with lower X-ray surface flux. They also found cold filamentary structures matching the $H\alpha$ emission and with high extinction regions seen on the optical extinction maps. This indicates a cooling mechanism generated by dust (Pandge et al. 2012). On the same work, they reported that a harder ionizing source is required to maintain such a high degree of ionization and that most of the jet power is mechanical. Gomes et al. (2016), using CALIFA datacubes, classified this object as type ii ETG.

A7 UGC 08234

This galaxy is part of a galaxy group and possesses a spiral companion, UGC 08237 (Nilson 1973). Gomes et al. (2016) classified this object as type ii ETG. There are no X-ray or radio properties reported in the literature. Its APO spectrum is dominated by stellar population, characterized by intense absorption bands and absence of emission lines.

APPENDIX B: EMISSION LINE FLUXES

In the optical region, according to Baldwin et al. (1981, BPT), the line ratios $[O III] \lambda 5007 \text{ \AA} / H\beta$ and $[N II] \lambda 6583 \text{ \AA} / H\alpha$ can be used to classify the excitation mechanism that powers the optical lines based on the position of the points in the diagram. After running the stellar population synthesis for the SDSS spectra, we subtracted the

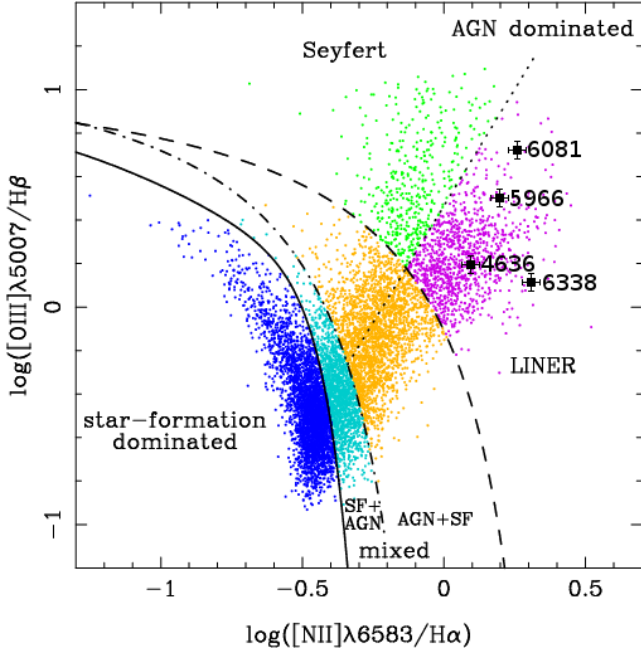


Figure B1. BPT diagram for the galaxies with optical spectra. The number of the NGC catalog is shown on the right side of each point. The points were plotted over the diagram from Bamford et al. (2008)

Table B2. Optical emission line fluxes in units of 10^{-15} ergs/s/cm 2 .

Object	H β 4861	[OIII] 5007	[NII] 6549	H α 6563	[NII] 6585	[SII] 6718	[SII] 6732
NGC 4636	1.9	2.7	3.43	6.84	8.77	3.48	3.10
NGC 5966	0.87	2.26	1.75	2.69	3.92	2.79	2.00
NGC 6081	1.05	3.7	7.26	6.73	13.5	5.61	3.71
NGC 6338	1.82	2.38	4.37	5.43	11.5	3.99	2.87

stellar component and measured the emission line fluxes by fitting gaussians to the emission lines. Although there are still controversies on individual objects (e.g. Martins et al. 2012, who found a galaxy with no signs of activity but whose line ratios put it as a Seyfert galaxy), these diagrams can be used with great confidence to study the nature of the central source that powers the observed emission lines.

The emission line fluxes measured in the galaxy sample are listed in Table B2 and their ratios are plotted in Figure B1. From the locus of points occupied by our targets, we confirm the LINER nature of the galaxies. Only NGC 4636 and NGC 5966 had already been previously classified as LINER (Véron-Cetty & Véron 2006; Kehrig et al. 2012). The results obtained allow us to state that our sample is composed of 5 ETGs with LINER emission, 1 spiral galaxy and 1 ETG with no data about its emission lines.

This paper has been typeset from a T $_E$ X/L $_A$ T $_E$ X file prepared by the author.